Late Cretaceous – early Eocene counterclockwise rotation of the Fueguian Andes and evolution of the Patagonia-Antarctic Peninsula system

Fernando Poblete, Pierrick Roperch, Cesar Arriagada, Gilles Ruffet, Cristobal Ramírez de Arellano, Francisco Hervé, Marc Poujol

Late Cretaceous – early Eocene counterclockwise rotation of the Fueguian Andes and evolution of the Patagonia-Antarctic Peninsula system

F. Poblete[a, b,*], P. Roperch[b], C. Arriagada[a], G. Ruffet[b], C. Ramírez de Arellano[c], F. Hervé[a, c,]., M. Poujol[b]

[a] *Departamento de Geología, Universidad de Chile, Santiago, Chile*

[b] *CNRS (CNRS/INSU) UMR 6118, Géosciences Rennes, 35042 Rennes Cedex, France and Université de Rennes I, Géosciences Rennes, 35042 Rennes Cedex, France*

[c] *Carrera de Geología, Universidad Andres Bello, Salvador Sanfuentes 2375, Santiago, Chile.*

[*] Corresponding author (F. Poblete, Géosciences Rennes, campus de Beaulieu, 35042, Rennes, France; e-mail: ferpoble2@gmail.com)

Abstract

The southernmost Andes of Patagonia and Tierra del Fuego present a prominent arc-shaped structure: the Patagonian Bend. Whether the bending is a primary curvature or an orocline is still matter of controversy. New paleomagnetic data have been obtained south of the Beagle Channel in 39 out of 61 sites. They have been drilled in Late Jurassic and Early Cretaceous sediments and interbedded volcanics and in mid-Cretaceous to Eocene intrusives of the Fuegian Batholith. The anisotropy of magnetic susceptibility was measured at each site and the influence of magnetic fabric on the characteristic remanent magnetizations (ChRM) in plutonic rocks was corrected using inverse tensors of anisotropy of remanent magnetizations. Normal polarity secondary magnetizations with west-directed

declination were obtained in the sediments and they did not pass the fold test. These characteristic directions are similar to those recorded by mid Cretaceous intrusives suggesting a remagnetization event during the normal Cretaceous superchron and describe a large (>90°) counterclockwise rotation. Late Cretaceous to Eocene rocks of the Fueguian Batholith, record decreasing counterclockwise rotations of 45° to 30°. These paleomagnetic results are interpreted as evidence of a large counterclockwise rotation of the Fueguian Andes related to the closure of the Rocas Verdes Basin and the formation of the Darwin Cordillera during the Late Cretaceous and Paleocene.

The tectonic evolution of the Patagonian Bend can thus be described as the formation of a progressive arc from an oroclinal stage during the closure of the Rocas Verdes basin to a mainly primary arc during the final stages of deformation of the Magallanes fold and thrust belt. Plate reconstructions show that the Antarctic Peninsula would have formed a continuous margin with Patagonia between the Early Cretaceous and the Eocene, and acted as a non-rotational rigid block facilitating the development of the Patagonian Bend.

1.0 Introduction

An impressive feature of the Patagonia-Antarctic Peninsula system is the striking opposite curved shape between the Patagonian Bend (Fig. 1), where the main structures and physiographic features change from a N-S trend in southern Patagonia to a ESE-WNW orientation in Tierra del Fuego, and the northern tip of the Antarctic Peninsula with an inversed shape (Fig. 1). Wegener (1929) first described this major structure and proposed that South America and the Antarctic Peninsula were joined at their tip and that the

orogenic curvature of Patagonia resulted from westward drift of South America. Although nearly a century has passed since his insightful work, the tectonic evolution of the two regions during Gondwana breakup and the possible oroclinal bending of the southernmost South America (Carey, 1958) are still a matter of controversy (Fig. 2).

Similar geologic features between southernmost America and the Antarctic Peninsula (Dalziel et al., 1975; Hathway, 2000; Hervé et al., 2005; Katz and Watters, 1966) suggest that they have been connected. However, the initial geometrical arrangement of these two units has been intensely debated: while some paleogeographic reconstructions suggest that the Antarctic Peninsula was a straight prolongation of Patagonia, forming a rectilinear margin during the Gondwana breakup (Fig. 2a) (Dalziel et al., 1973; Storey, 1991; Suárez and Pettigrew, 1976), others place the Antarctic Peninsula at the western edge of Patagonia (Fig. 2b) (Dalziel et al., 2013; Ghidella et al., 2002; Harrison et al., 1979; König and Jokat, 2006; Miller, 1983). The possible oroclinal bending of the southern margin of the Andes has also been debated. Counterclockwise (CCW) tectonic rotations recorded in the Fueguian Andes were interpreted as evidence for an oroclinal bending of the Patagonian Bend related to the closure of the Rocas Verdes Basin (Fig. 2a,b) (Burns et al., 1980; Cunningham et al., 1991; Dalziel et al., 1973). But, recent studies have suggested that the curved margin of southernmost South America is a primary feature (Diraison et al., 2000; Ghiglione and Cristallini, 2007; Ramos and Aleman, 2000).

Paleomagnetic studies in Patagonia and the Antarctic Peninsula offer a powerful tool to constrain paleogeographic reconstructions and the origin of the curvatures. As an example, a straight margin of Patagonia would restrict a western position of the Antarctic Peninsula during the early stage of Gondwana breakup while a counterclockwise rotation of

Patagonia and a clockwise rotation of the Antarctic Peninsula have been invoked to explain the closure of the Rocas Verdes basin and the development of the Scotia Arc region (Dalziel and Elliot, 1972; Torres Carbonell et al., 2014). Paleomagnetic data have already ruled out the possible clockwise rotation of the Antarctic Peninsula (at least since mid-Cretaceous) (Grunow, 1993; Poblete et al., 2011; Watts et al., 1984), whereas in Patagonia the available paleomagnetic data suggest oroclinal bending of the southermost part of the forearc (Burns et al., 1980; Cunningham et al., 1991; Dalziel et al., 1973) and very minor or no rotations in the Magallanes Fold and Thrust Belt (FTB) (Maffione et al., 2010; Poblete et al., 2014). However, in Patagonia paleomagnetic data remain scarce and sometimes questionable (Poblete et al., 2014; Rapalini, 2007) and, they do not permit to discard the hypothesis that vertical axis rotation could be related to strike-slip tectonics (Cunningham, 1993; Cunningham et al., 1991; Diraison et al., 2000).

We present a paleomagnetic study from 61 sites, sampled in the Early Cretaceous-Eocene Fueguian Batholith and in Early Cretaceous sediments and volcanic rocks from the Fueguian Archipelago (Fig. 3a and 3b). We used these new data and already published ones to constrain the evolution of the Patagonian Bend and its relation to the Antarctic Peninsula in paleogeographic reconstructions.

2.0 Tectonic setting and geological evolution

2.1 Present-day geodynamic configuration

Southernmost Patagonia belongs to the Scotia plate, which is bounded to the South American plate through the North Scotia ridge and the Magallanes Fagnano fault zone (MFFZ) (Klepeis, 1994a; Lodolo et al., 2003; Smalley et al., 2003), and to the Antarctic

plate by the South Scotia ridge and the Shackleton Fracture Zone (SFZ) (Klepeis and Lawver, 1996; Smalley et al., 2007) (Fig. 1). Earthquake slip vectors and focal mechanisms show left-lateral strike-slip motion in both the North and South Scotia ridges (Smalley et al., 2007).

2.2 Geological Evolution

The extension associated with Gondwana breakup resulted in the generation of silicic volcanism in Patagonia during the Jurassic (Pankhurst et al., 2000) and the Early Cretaceous (Calderón et al., 2007). Subaqueous pyroclastic flows, tuff and rhyolites of the Tobífera Formation are vestiges of this volcanism (Bruhn et al., 1978; Wilson, 1991). The continuation of the extension led to the development of the Rocas Verdes basin (Fig. 2) and the formation of oceanic crust during the Late Jurassic (Calderón et al., 2007; Mukasa and Dalziel, 1996) which is preserved today as the ophiolitic Tortuga and Sarmiento complexes and associated outcrops south of 51° S (Fig. 3a-b). It consists of pillow lavas, dykes and gabbros that have been interpreted as the upper sequence of the ophiolite (Dalziel et al., 1974; Stern and De Wit, 2003). Filling the basin is the Yahgan formation (Fig. 3a-b), an Upper Jurassic- Lower Cretaceous sequence (Barbeau et al., 2009; Calderón et al., 2007; Katz and Watters, 1966; Klepeis et al., 2010) of greywackes and dark grey argillites intercalated with volcanic breccias and conglomerates (Katz and Watters, 1966; Suárez et al., 1985) which was deformed during the mid-Cretaceous (Halpern and Rex, 1972). The sedimentary rocks interlace westward with the latest Jurassic-Early Cretaceous volcanic arc deposits of the Hardy Formation (Fig. 2, 3a-b) suggesting that calc-alkaline arc volcanism was coeval to back-arc magmatism and sedimentary infilling (Katz and Watters, 1966; Miller et al., 1994).

Mid-Cretaceous crustal shortening resulted in the collapse of the Rocas Verdes basin which was likely controlled by a first event of obduction at ~86 Ma (Klepeis et al., 2010) and underthrusting of the South American continental crust at ~9 Kbar (Maloney et al., 2011). Paleozoic schist basement and rift related sequences of the Cordillera Darwin metamorphic complex (Fig. 3a) registered this phase of contraction (Klepeis et al., 2010). Coinciding with obduction, crustal loading and shortening marked the onset of the Magallanes foreland basin and of the Magallanes FTB (Fig. 3a). Deposits of the early Late Cretaceous Punta Barrosa Formation in Última Esperanza and Cerro Matrero Formation in Tierra del Fuego recorded the initial stages of the Magallanes basin (Cortés and Valenzuela, 1960; Fildani et al., 2003; Fosdick et al., 2011; McAtamney et al., 2011). Rapid exhumation of the Cordillera Darwin during the Paleogene (Gombosi et al., 2009; Kohn et al., 1995; Nelson, 1982) coincides with advance of the FTB into the Magallanes foreland (Alvarez-Marrón et al., 1993; Klepeis, 1994b).

The South and Fueguian batholiths (southern parts of the extensive Patagonian Batholith) rim the Rocas Verdes basin (Fig. 2, 3), and consist of Late Jurassic peraluminous leucogranites and Early Cretaceous-Cenozoic gabbros and granitoids (Bruce et al., 1991; Hervé et al., 2007; Hervé et al., 1984). While the geochemical and petrochemical data suggest a subduction origin for Cretaceous-Cenozoic magmatism (Bruce et al., 1991; Hervé et al., 2007; Suárez et al., 1985), they do not clearly establish whether the Late Jurassic magmatism were formed in a subduction related arc or if they result of extension (Hervé et al., 2007).

3.0 Geology and paleomagnetic sampling

The paleomagnetic sampling is summarized in Table AM_01 (auxiliary material) and organized according to the rock type. Sixty-one sites were sampled of which twelve were drilled in sedimentary and volcaniclastic rocks; four were drilled in sills at Dientes de Navarino that intrude the sediments of the Yahgan formation; four were drilled in pillow lavas and dikes from the ophiolitic complexes and thirty-nine in intrusive rocks. Two sites combine samples drilled in intrusive and sedimentary or volcanic rocks. All samples were cored with a portable drill and oriented by sun or magnetic compass. Magnetic orientations were corrected using the declination calculated from the International Geomagnetic Reference Filed at each site. Radiometric age control is based on a compilation of previously published ages (see Table AM_01 for references) and new $^{39}Ar/^{40}Ar$ and laser ablation ICP-MS U-Pb ages.

3.1 Sedimentary and volcanic rocks

All sites were drilled on Navarino Island and Hardy Peninsula (Hoste Island) except CB30 that was drilled in the Ballenero Channel, (Figs. 3a&3b). Nine sites from the Yahgan Formation were sampled. Four sites (TU49, TU50, TU51, TU52), located near the Murray Channel (northwest corner of Navarino Island), were drilled in deformed fine-grained sandstones and mudstones of the Wulaia member. Two sites (TU84, TU87) were sampled at Dientes de Navarino in less deformed fine-grained sandstones and mudstones of the Wulaia member. Two sites were drilled in greenish sandstones of the Bahía Douglas member (TU53 in the south-west coast of Navarino Island and TU57 in the Hardy Peninsula) and one site (TU56) in clasts of intrusive rocks of the Cretaceous conglomerate known as the Tekenika beds (Dott et al., 1977).

Four sites were sampled in rocks from the Hardy Formation. The sites TU59, TU60 and TU61 were drilled in greenish volcaniclastic rocks at Hardy Peninsula but at different localities from those sampled by Cunningham et al. (1991) (Fig. 3b). Site CB30 (Fig. 3a) was drilled at Ballenero Channel (~200 Km to the west of sites TU59, TU60, TU61) and consists of an intercalation of greenish volcaniclastic and rhyolitic rocks intruded by decametric undated sills, which were also sampled.

3.2 Ophiolitic rocks

Sites TU54 and TU63 were drilled in the Tortuga Ophiolite (Fig. 3b). Site TU54 was drilled in very well preserved pillow lavas (where a bedding attitude was determined) and TU63 in intrusive rocks. Site CB05 was drilled in the south shore of the Beagle Channel (Dumas Peninsula, Fig. 3b) in gabbros intruded by aphanitic mafic rocks. Finally, site TU81 (the northernmost site) was drilled in pillow lavas attributed to the Rocas Verdes basin floor and is located close to the trace of the Magallanes Fagnano fault zone.

3.3 Intrusive rocks

The Late Jurassic-Eocene Fueguian Batholith (Barbeau et al., 2009; Hervé et al., 1984; Klepeis et al., 2010; Suárez et al., 1985) is located in what is now the Scotia Plate (Hervé et al., 2007) (Fig. 1 and 3a). While most of the intrusive rocks crop out to the southwest of the Rocas Verdes basin, isolated bodies located in the eastern part of the Beagle Channel have been attributed to rear-arc magmatism (Gonzáles-Guillot et al., 2011) (Fig. 3b).

Intrusive bodies were sampled in Navarino Island and in Dumas and Hardy Peninsula (Fig. 2b). In Navarino Island four sites (TU82, TU83, TU85 and TU86) were sampled in >100m thick sills at Dientes de Navarino (Katz and Watters, 1966) which were also sampled by Burns et al. (1980). A pyroxene K/Ar age of 115 ± 5 Ma was obtained by Burns et al. (1980), with low precision due to low potassium content of the mineral. Katz and Watters (1966) and Burns et al. (1980) indicated that the country rock sediments were probably intruded by the sills prior to folding. One site (TU89) was drilled in the Late Cretaceous Castores intrusive (Suárez et al., 1985). Finally, site TU88 was drilled in the Late Cretaceous Santa Rosa intrusive (Suárez et al., 1985).

Six sites were sampled in an early Late Cretaceous large intrusive (Hervé et al., 1984; Suárez et al., 1985) located in the northeast corner of Dumas Peninsula (Fig. 3b). Lithologies vary from granodiorites to tonalites. Sites TU64 and CB01 presented a subvertical ~E-W oriented foliation with elongated mafic enclaves; site CB03 was sampled in the contact between the intrusive and the Yahgan formation where the host rock (Yahgan Formation) was also sampled; sites CB02, CB04 and CB06 do not show evidence of foliation.

The Fueguian Batholith forms a NW-SE-trending belt along the south-west Pacific shore. In Hardy Peninsula, site TU55 was sampled in a Paleocene tonalite pluton and site TU62 in a small granodiorite body both without evidence of foliation. Nine sites were sampled in the southern arm of the Beagle Channel (Fig. 3b). Site CB07 was sampled in a granodiorite with a faint foliation while the site CB08 was sampled in a horblendite cut by pegmatitic dikes of the same composition. A middle Cretaceous K/Ar age in amphibole was reported near the sites (Suárez et al., 1985). To the west, site CB09 was drilled in a micro

gabbro-diorite cut by quartz-feldspar veins. Site CB10, located 0.6 Km to the south of site CB09, was drilled in a hornblende-biotite granite with mafic enclaves of irregular shapes and sizes. Sites CB11, CB12 and CB13 were drilled 10 Km to the west of the site CB09. Site CB11 was drilled in a tonalite with mafic enclaves whereas the sites CB12 and CB13 were drilled in a gabbro-diorite. Finally, sites CB14 and CB15 were drilled in a tonalite located in the western side of Hoste Island.

Fourteen sites were sampled in the area of Ballenero and O'Brien Channels (to the west of the western end of the Beagle Channel, Fig. 3a). Samples from site CB16 were drilled in a granitic intrusive and a mafic dike that cuts the granite. Gabbros and hornblendites (Hervé et al., 1984; Suárez et al., 1985) were sampled at sites CB17, CB18 and CB20 while site CB19 was drilled in a coarse grain granite. To the west, site CB21 was sampled in a horblendite, sites CB22, CB23, CB24 and CB25 in a tonalite and site CB26 in a granite. Published datings near these sites suggest a middle Cretaceous age for these rocks (Hervé et al., 1984; Suárez et al., 1985). Finally, sites CB28 and CB29 were drilled in a granite and a granodiorite of probably Paleocene age (Suárez et al., 1985) and site CB27 was drilled in a mafic dike intruding the plutonic rocks at site CB28.

Six sites were drilled in the area of Brecknock and Rolando Peninsula (Fig. 3a). Sites CB31, CB32 and CB33 were drilled in a late Paleocene tonalite. To the north, sites CB34, CB35 and CB36 were sampled in an undated granodiorite cut by dikes (Fig. 3a). Site CB37 (north of Rolando Peninsula) was drilled in a middle Cretaceous foliated diorite immediately south of the trace of the Magallanes Fagnano fault zone (Fig. 3a).

4.0 Geochronological constrains: New $^{40}Ar/^{39}Ar$ and U-Pb data

4.1 $^{40}Ar/^{39}Ar$ methodology

Nine paleomagnetic specimens (from sites CB08; CB09, CB12, CB13, CB15, CB19, CB20, CB21, CB33) were analyzed by continuous CO_2 laser probe stepwise heating $^{40}Ar/^{39}Ar$ technique at Géosciences Rennes (see auxiliary material Table AM_02).

The selected minerals were wrapped in Al foil to form small packets (11 × 11 mm) that were stacked up to form columns within which packets of fluence monitors were inserted every 10 samples. Irradiations was performed at the McMaster reactor (Hamilton, Canada) using medium flux location (8E) with Cd-shielding and lasted 127.37 hr (J/h ≈ $4.75x10^{-5}$ h^{-1}). Irradiation standard was sanidine TCRs (28.608 ± 0.033 Ma according to Renne et al. (1998) and Renne et al. (2011). The sample arrangement within the irradiation allowed us to monitor the flux gradient with a precision of ± 0.2 %.

Heating steps were performed with a CO_2 laser probe. All experiments concerned single grains. The experimental procedure was described by Ruffet et al. (1991) and Ruffet et al. (1995). The five argon isotopes and the background baselines were measured in eleven cycles, in peak-jumping mode. Blanks were performed routinely each first or third/fourth run, and subtracted from subsequent sample gas fractions. All isotopic measurements are corrected for K, Ca and Cl isotopic interferences, mass discrimination and atmospheric argon contamination.

Apparent age errors are plotted at the 1σ level and do not include the errors on the $^{40}Ar^*/^{39}Ar_K$ ratio and age of the monitor and decay constant. The errors on the $^{40}Ar^*/^{39}Ar_K$ ratio and age of the monitor and decay constant are included in the final calculation of the

(pseudo-)plateau age error margins or for apparent ages individually cited. Analyses were performed on a Map215® mass spectrometer.

It is commonly considered that a plateau is obtained when calculated $^{40}Ar^*/^{39}Ar_K$ ratios of at least three consecutive steps, comprising a minimum of 70 % of the ^{39}Ar released, agree within 1 or 2σ error bars with the weighted mean calculated $^{40}Ar^*/^{39}Ar_K$ ratio of the plateau segment. Pseudo-plateau ages can be defined with less than 70% of the ^{39}Ar released. All ages are displayed at the 1σ level.

Analytical data and parameters used for calculations (isotopic ratios measured on K, Ca and Cl pure salts; mass discrimination; atmospheric argon ratios; J parameter; decay constants, etc.) and reference sources are available in Table AM_02, auxiliary material.

4.2 $^{40}Ar/^{39}Ar$ results and comparison with previous ages

Six of the nine analyzed samples (Fig. 4) yielded age spectra allowing a plateau age calculation. Suárez et al. (1985) report an extensive set of K/Ar rock ages in the area of Hoste and adjacent islands. Near sites CB07 and CB08, they reported two amphibole K/Ar ages of 108 ± 5 Ma and 110 ± 2 Ma from a gabbro (gabbroic assemblage from Hervé et al. (1984)), which probably would have to be recalculated with the presently used decay constants. The new amphibole $^{40}Ar/^{39}Ar$ analysis in sample CB08 (Hornblendite, south arm of Beagle Channel) yields a plateau age at 102.0 ± 0.4 Ma, validated by inverse isochron analysis (Hanes, 1985; Roddick et al., 1980; Turner, 1971) with an isochron age at 101.8 ± 0.4 Ma ($(^{40}Ar/^{36}Ar)_i$ = 309.2 ± 7.5), which confirms the middle Cretaceous age reported for the intrusive by Suárez et al. (1985).

Gabbros also crop out in the south shore of the south arm of the Beagle Channel and were initially grouped in a single gabbroic assemblage of Early Cretaceous (141 to 103 Ma) ages (Hervé et al., 1984). New $^{40}Ar/^{39}Ar$ analyses performed on samples CB09 (amphibole and biotite) and CB13 (amphibole) collected from intrusives of the gabbroic assemblage provide plateau and pseudo-plateau ages at ca. 66 Ma (Fig. 4). These results indicate that gabbros emplacement occurred not only in the early Cretaceous as suggested by Hervé et al. (1984) but also close to the Cretaceous-Paleogene boundary. This phase of magmatic activity is also evidenced by an amphibole from tonalite sample CB15 (south arm of the Beagle Channel) which yields a pseudo-plateau age at ca. 67.6 Ma (Fig. 4). Saddle shaped age spectra of amphiboles CB13 and CB15 could express an excess argon contamination. In such case, saddle minima are maximum estimates of the true age of analyzed material. Nevertheless, isochron analyses yield ages fully concordant with calculated pseudo-plateau ages in both cases, suggesting that they are the best estimate of the cooling age of amphiboles. On the other hand, step heating procedure did not allow full separation of radiogenic and excess argon components within amphibole CB12 and the minimum apparent age (ca. 69.3 Ma, Table AM_02) of saddle shaped age spectrum is only a maximum estimate of the cooling age of the mineral.

In Canal Ballenero, amphibole CB19 (granite) $^{40}Ar/^{39}Ar$ plateau age at ca. 58.7 Ma confirms the Paleocene age proposed by Suárez et al. (1985). The biotite experiment, despite a slight hump shape characteristic of ^{39}Ar recoil related to chloritization (Ruffet et al., 1991), yields apparent ages globally concordant with amphibole ones, validating proposed late Paleocene cooling age. On the other hand, despite disturbed age spectra precluding any plateau age calculation, observed apparent ages measured on amphiboles

from samples CB20 (hornblende gabbro) and CB21 (gabbro) suggest that they could be early to middle Cretaceous. CB20 hump-shaped age spectrum probably expresses a disturbance related to Paleocene granitic intrusion (granite CB19 was collected at 300 m of gabbro CB20).

Fully concordant plateau ages of ca. 53.6 Ma calculated for amphibole and biotite from sample CB33 (tonalite) are younger than the age previously assigned on the map (SERNAGEOMIN, 2003) supporting the hypothesis of a local oceanward shift of plutonism during the Paleocene – early Eocene (Hervé et al., 1984). $^{40}Ar/^{39}Ar$ ages confirm unpublished U-Pb ages (Hervé personal comm.) on plutonic units located 5 km to the west.

4.3 New U-Pb ages

Zircon grains were extracted from two large samples from site CB01 and CB07 following standard mineral separation methods. After crushing and milling, zircons from three fractions below 250 µm (<90 µm; 90-125 µm and 125-250 µm) were separated independently by panning and hand peaking to avoid loss of small zircons. Separation was carried out in the Solid Analysis Laboratory of University Andrés Bello. The grains were then hand-grounded and polished before being imaged by cathodoluminescence (CL) using a Reliotron CL system equipped with a digital color camera available in Géosciences Rennes.

U-Pb geochronology of zircon was conducted by in-situ laser ablation inductively coupled plasma mass spectrometry (LA-ICPMS) at Géosciences Rennes using a ESI NWR193UC exciter laser coupled to a quadripole Agilent 7700x ICP-MS. A complete description of the analytical procedure can be found in Ballouard et al. (2015). Single

analyses consisted of 20 s of background integration followed by 60 s integration with the laser firing and then a 10 s delay to wash out the previous sample. Ablation spot diameters of 25 µm with repetition rates of 3 Hz and a fluence of 9 J/cm^2 were used. Data were corrected for U–Pb and Th–Pb fractionation and for the mass bias by standard bracketing with repeated measurements of the GJ-1 zircon (Jackson et al., 2004). Along with the unknowns, the zircon standard Plešovice (337.13 ± 0.37 Ma, Sláma et al. (2008)) was measured to monitor precision and accuracy of the analyses and produced a concordia age of 336.8 ± 2.6 Ma (MSWD=0.92, n=9). Data reduction was carried out with the GLITTER® software package developed by the Macquarie Research Ltd. Concordia ages and diagrams were generated using Isoplot/Ex (Ludwig, 2001). All errors given in auxiliary material Table AM_02b are listed at one sigma, but where data are combined for regression analysis, the final results are provided with 95% confidence limits.

For sample CB01 (Tonalite, Murray Channel), 17 zircon grains were analyzed (see auxiliary material Table AM_02b). They present variable Pb (3-19 ppm) and uranium (170-1185 ppm) contents and their Th/U ratios between 0.62 and 1.48 are consistent with their magmatic origin. Plotted in a Tera-Wasserburg concordia diagram (Fig. 4) they plot in a concordant position and define a concordia age (Ludwig, 1998) of 90.24 ± 0.75 Ma (MSWD=1.8), interpreted as crystallization age.

Nineteen zircon grains were analyzed for sample CB07 (granodiorite, west of site CB01) (see auxiliary material Table AM_02b). Their Pb contents vary from 7.7 to 25.5 ppm while their U contents are bracketed between 487 and 1539 ppm. Their Th/U ratios are typical for magmatic zircons with values between 0.36 and 0.85. They all plot in a

concordant position (Fig. 4) and allow calculation of a concordia age of 99.33 ± 0.67 Ma (MSWD=1.4) interpreted as their crystallization age.

5.0 Paleomagnetism

5.1 Paleomagnetic methodology

Natural remanent magnetization (NRM) was measured with a 2G cryogenic magnetometer (Université de Rennes 1, France) or with a Molspin (Universidad de Chile). Then, most samples were progressively demagnetized using thermal or stepwise alternating field (AF) methods in a shielded room and the magnetization was measured with the 2G magnetometer. The magnetic carriers of the characteristic remanent magnetization (ChRM) were further investigated by means of isothermal remanent magnetization (IRM) acquisition curves, thermal demagnetization of three axis-orthogonal IRMs, variation of low-field magnetic susceptibility versus temperature (K-T experiments) and hysteresis cycles (obtained with the AGM2900 from Princeton Measurements Corporation at LSCE, Gif/Yvette, France). Paleomagnetic and magnetic experimental procedures are described in more detail in Poblete et al. (2014). Polished thin sections of the studied rocks were observed in transmitted and reflected light and analyzed with a TESCAN scanning electron microscope (SEM) at Universidad Andrés Bello, Chile.

Anisotropy of magnetic susceptibility (AMS) of one or two specimens per core was measured with the KLY3 Agico spinner kappabridge.

In order to test the importance of the deviation of the remanent magnetization from the magnetic fabric, the determination of the anisotropy of remanent magnetization was

performed on several specimens per site from sites with high anisotropy of magnetic susceptibility. Anisotropy of anhysteretic remanent magnetization (AARM) was acquired along x/-x, y/-y, z/-z axes using DC fields of 60µT and AC fields between 60mT and 80mT. This procedure enables the removal of a residual NRM component and a possible contribution of a gyroremanent magnetization. Full thermoremanent magnetizations (TRM) were given along x/-x, y/-y, z/-z axes to determine the tensor of anisotropy of TRM (ATRM). Specimens were heated up to 600°C and cooled under a DC magnetic field of 60 µT. Three full TRMs acquired along the x, y and z axes are sufficient to determine the tensor of TRM anisotropy. With the six TRM acquisitions along x/-x, y/-y, z/-z, it was possible to estimate chemical changes from the variation in the intensity of the magnetization between two successive measurements along the same directions of magnetic changes (rx,ry,rz). For a few samples, the changes between two heating steps were greater than 5%. For these samples only, the effect of chemical changes were corrected using the variation in the intensity of the TRMs between 2 steps along the same axis and a medium rate of change was used in between step -x/y and between steps -y/z. The anisotropy corrected ChRM vector corresponds to the product of the in situ ChRM vector with the inverted tensor of ATRM or AARM.

5.2 Paleomagnetic Results

Site-mean ChRM directions were determined for thirty-nine of the sixty-one sites (Table 1). In some samples of sites labeled as TU, the NRM was measured in Chile prior to shipping the samples to France for their demagnetization and measurement with the 2G cryogenic magnetometer. The difference between the NRM measured in Chile and France (Fig. AM_01) indicates that a random spurious component of magnetization was acquired

during transport. However, it was easily removed (Fig. AM_01) after applying an alternating field at 5 or 7.5 mT. For these samples, an AF demagnetization at 7.5 mT was systematically performed prior to the thermal demagnetization.

5.2.1 Sediments, interbedded volcanic and ophiolitic rocks

ChRM directions were determined at five sites in sedimentary and volcaniclastic rocks and two sites in the ophiolitic rocks. The ChRM has negative inclination with a declination to the west in in situ coordinates. The ChRM was determined with intermediate to high unblocking temperatures (between ~350°C and ~580°C, Fig. 5a). In the Yahgan Formation, only the two most southern sites (TU53 and TU57) provided well-defined directions with $\alpha 95$ of 6.2° and 5.1°. Unstable magnetizations were found in samples from sites near the Beagle Channel. These sites were drilled in mudstones of the Wulaia member of the Yahgan Formation and they present evidence of cleavage that could explain the poor paleomagnetic record. Samples drilled in the Hardy Formation show very well defined univectorial magnetizations of normal polarity going through the origin (Fig. 5a) and a site-mean ChRM was determined for the three sites (TU59, TU60, TU61). We were able to obtain ChRMs of normal polarity at the sites TU54 (Fig. 5b) and TU63. Samples from two others sites attributed to the Rocas Verdes ophiolite (sites CB05 and TU81) provided well-defined ChRM directions for individual samples but the scatter observed at site level precludes further interpretation (see auxiliary material Fig. AM_02).

ChRM components obtained in sediments, volcanic and in one site of pillow lavas are well grouped in *in situ* coordinates while they are scattered after bedding correction (Fig. d5e). A similar observation was made by Cunningham et al. (1991). The fold test

(Tauxe and Watson, 1994) (Fig. 5f) based on our new data and those of Cunningham et al. (1991), confirms the secondary origin for the ChRMs.

K-T experiments showing Curie temperatures of ~320°C, and thermal demagnetization of orthogonal IRMs with unblocking temperatures below 320°C demonstrate that the main magnetic carrier for sedimentary sites near the Beagle Channel is pyrrhotite (see auxiliary material Fig. AM_03a). Pyrrhotite is also observed in the pillow lavas at site TU54 (Fig. 5b-c, see auxiliary material Fig. AM_03b). In contrast, high unblocking temperatures (550-580°C) of the ChRM for samples from sites in the Peninsula Hardy (Fig. 5a) indicate that magnetite or Ti-poor titanomagnetite is the main magnetic carrier. Thermal demagnetizations of three-component IRM (Lowrie, 1990) show an abrupt drop of the soft and medium coercivity fractions around 550-580 °C (see auxiliary material Fig. AM_04a) and K-T experiments confirm that titanomagnetite and magnetite are the main magnetic carriers in samples from Yahgan and Hardy Formation. At site TU61, secondary magnetite growing in veinlets were found in SEM data (see auxiliary material Fig. AM_04b), supporting a secondary origin for the magnetization as already pointed out by Cunningham et al. (1991). Calderón et al. (2013) suggested that a burial non-deformative metamorphism converted the primary mineralogy of the ophiolites to low- to intermediate-grade metamorphic assemblages formed during ocean-floor type alteration in a suprasubduction setting. However, sediments from the northern part of Navarino Island are foliated and pyrrhotite is part of the mineralogy. Remagnetization is likely associated with metamorphism but burial metamorphism due to a thick overlying turbiditic sequence is not the main or single cause of this remagnetization.

At Dientes de Navarino (K/Ar age of ~115 Ma (Burns et al., 1980; Suárez et al., 1985)), ChRMs of normal polarity (Fig. 5d, g) were determined at sites TU82, TU83, TU85, TU86 in the sills previously studied by Burns et al. (1980). In in situ coordinates (Fig. 5g), the ChRMs are similar to directions found in remagnetized rocks: dec: 258.8°, inc: -73.2, α95: 9.7°. The sills are intruding the sedimentary sequence which has a dip toward the S-SW (strike of 107° and dip of 45°). After applying the tilt correction (using the strike and dip of the sediments), the mean direction (dec: 353.7°, inc: -50.8°, α95: 9.7°) has low inclination and a north oriented declination (Fig. 5g). Katz and Watters (1966) and Burns et al. (1980) considered it unlikely that the thick series of dolerites intruded the sediments after folding. This result in addition with the low inclination found after the tilt correction suggests that the magnetization was acquired after folding. This interpretation implies that the magnetization is not of primary origin. Unfortunately there is no fold test available for the sills. Observations of thin sections under an optical microscope confirm the alteration due to low-temperature metamorphism within the sills reported by Katz and Watters (1966). Two sites were sampled in sediments and one site provided ChRM carried by pyrrhotite with a mean direction close to the one recorded by the sills despite some internal scatter (low Fisher concentration parameter). We thus consider that the ChRMs recorded in Dientes de Navarino sills are likely of secondary origin and acquired at the same time than the remagnetization in Peninsula Hardy.

CB30 is the westernmost site drilled in the Hardy formation. Two components of magnetization of normal and reverse polarity were found but the tilt corrected directions have low inclinations (Table 01) indicating a most probable secondary magnetization.

5.2.2 Intrusive rocks

At most sites, high magnetic susceptibilities (see Auxiliary Material Table AM_01 and Fig. AM_05) and K-T experiments (see Auxiliary Material Fig. AM_06a) indicate that magnetite is the main magnetic mineral with a small amount of maghemitization in some samples shown by a drop in magnetic susceptibility around 350 °C. High ratios of Bcr/Bc and low ratios of Mrs/Ms (see Auxiliary Material Table AM_03 and Fig. AM_06b) indicate the presence of large multidomain grains of magnetite. Fortunately, at many sites fine-grained magnetite is also present in mafic minerals as observed in SEM images (see auxiliary material Fig. AM_07a). As it is frequently observed in intrusive rocks (Ferrando et al., 2014; Parada et al., 2005), the most mafic intrusive rocks like the gabbros have stable remanent magnetization with intensity above 1 Am^{-1} (for example site CB08, CB12, Table AM_01 and Fig. AM_05), while diorite and granodiorite have less stable remanent magnetization.

Samples from a few sites (CB07; CB09; CB34; CB35; CB36) have low magnetic susceptibility and contain stable remanent magnetizations. Fine-grained magnetite is essentially the carrier of the remanent magnetization except at sites CB35 and CB36 where pyrrhotite is the main magnetic carrier of the ChRMs.

Very well defined ChRMs were obtained after thermal (Fig. 6a-b-c-d-e) or AF demagnetization. Thermal demagnetization is often more efficient to remove component of viscous origin and was used in most cases (Fig. 6d). Almost all sites have normal polarity ChRMs, except for the Paleocene sites CB09, CB10, CB11, CB12, CB13, CB15 (South Arm of the Beagle Channel) and for the sites CB16, CB18, CB20, CB30 (Ballenero Channel) and CB35-36 (Rolando Peninsula) (Table 01 and Fig. 6f).

Paleomagnetic results were also obtained on both sides of the Murray Channel (TU88, TU89 and CB01, TU64). K/Ar ages of ~85 Ma (Suárez et al., 1985) and our new U-Pb age of 90 Ma at site CB01 indicates magmatic emplacement at the end of the long normal Cretaceous superchron in agreement with the normal polarity recorded by these sites. Sites CB04 and CB06 presented unstable magnetization and yield no results.

Farther south in Peninsula Hardy, two sites (TU55; TU62) provided well-defined ChRMs.

In the southern arm of the Beagle Channel, well-defined ChRM directions of normal polarity were obtained at sites CB07 and CB08 (Bahia Fleuriais) (Fig. 6f) in agreement with the polarity expected for intrusive rocks with a $^{39}Ar/^{40}Ar$ age of ~102.2±0.4 Ma at site CB08 and an U-Pb age of 99.3±0.7 Ma at site CB07.

A reverse polarity magnetization was recorded by 6 sites (CB09-CB10-CB11-CB12-CB13-CB14-CB15). New $^{39}Ar/^{40}Ar$ ages for three of these sites are in the range 65-68 Ma (Fig. 4) and it is possible that these six sites record the same event of magmatic activity at the end of the Cretaceous.

Paleomagnetic directions in the area of Ballenero Channel (west of the Beagle Channel) are, for all sites but CB18 and CB20, of normal polarity (Fig. 6f) with well-defined ChRMs and 95% confidence angle lower than 9°. Sites CB21 and CB22 record the lowest inclinations.

Sites CB23, CB24, CB25 and CB26 do not provide well-defined characteristic directions. Site-mean directions of the Paleocene sites CB27, CB28 and CB29 (Ballenero

Channel) and sites CB32 and CB33 (Brecknock Peninsula) have all normal polarity magnetizations and are very well grouped with 95% confidence angle lower than 5° for all sites except site CB32 (8.3°). No ChRM was isolated at site CB31.

Farther north, at sites CB35 and CB36, a well-defined paleomagnetic direction of reverse polarity, carried by pyrrhotite, was observed in some samples of both sites. SEM observations confirm the presence of pyrrhotite as blebs trapped within mafic minerals (see auxiliary material Fig. AM_07b). Because of the low number of results at sites CB35 and CB36, we decided to combine the ChRMs of both sites in a single mean direction. These sites are within the Cretaceous belt of intrusives and the reverse polarity of the remanent magnetization indicates that the magmatic activity occurred before or after the normal Cretaceous superchron. Site CB34 has unstable magnetization. Only three samples provided stable magnetization for site CB37 but the very low inclination (~23°) suggests an undetected tilt and these few results are not considered.

In intrusive rocks, magnetic carriers located within other silicate minerals (magnetite, see Fig. AM_07a) or as blebs trapped within mafic minerals (pyrrhotite, see Fig. AM_07b) suggest that they were formed during magmatic crystallization (Bacon, 1989; Evans and McElhinny, 1966). We thus consider that the magnetization carried by pyrrhotite is of primary origin in the intrusive rocks. The very well-defined ChRMs and the agreement between the observed polarity and the radiometric age (i.e. mid-cretaceous rocks record a normal polarity) support a primary magnetization in intrusive rocks.

5.3 Magnetic fabric

Mean AMS results, ATRM versus AMS results, and AARM versus AMS results are summarized in Table AM_04a, b, c (see auxiliary material).

5.3.1 Magnetic fabric in sedimentary rocks

The highest degrees of anisotropy are found in the area of the Murray-Beagle Channel and the lowest values in the area of Dientes de Navarino and Hardy Peninsula (Fig. 7a, b)

In the Murray-Beagle Channel region (sites 49, 50, 51, 52), the axes of the AMS ellipsoids are very well grouped in *in situ* coordinates (Fig. 7c) but there is a substantial scatter of the principal axis of the AMS ellipsoids after bedding correction (see auxiliary material Fig. AM_08). This clearly demonstrates that the magnetic fabric is of tectonic origin and related to a pervasive WNW-ESE foliation of similar orientation than the tectonic foliation reported by Cunningham (1995), in the north arm of the Beagle Channel. The magnetic lineation is nearly vertical and this suggests that the magnetic fabric is of tectonic origin (Robion et al., 2007). Despite a low degree of anisotropy (Fig. 7b), the magnetic fabric recorded in the Tortuga pillow lavas (TU54) has the same orientation with steep lineation than the one recorded at site TU53 in sediments (Fig. 7c). Sediments at Dientes de Navarino (sites TU84, TU87) and Peninsula Hardy (TU57, TU59, and TU60) have an incipient tectonic fabric replacing the primary sedimentary fabric (Fig 7c). Low temperature metamorphism and remagnetization occurred likely during this stage of deformation.

5.3.2 Magnetic fabrics in intrusive rocks.

In the field, the sampled intrusive rocks do not show pervasive homogeneous tectonic foliation but many sites have a strong well-defined magnetic fabric that is likely a late-magmatic fabric related to strain during pluton emplacement. Most sites have high to very high magnetic susceptibility due to multidomain magnetite which control the AMS fabric.

In the four sites drilled in the intrusive rocks of Dientes de Navarino, the degree of anisotropy is very low (< 1.035) without preferential orientation of the axes of the AMS ellipsoids (See auxiliary material Table AM_04a).

Intrusive rocks near the intersection of the Beagle and Murray channels record high anisotropy degrees (Fig. 8a, b). Site TU88 was drilled in the small Santa Rosa pluton while site TU89 was drilled in the Castores pluton (Fig. 8a). The magnetic fabric is likely related to pluton emplacement rather than to the pervasive deformation previously described in sediments. This interpretation is supported by the concentric magmatic fabric around the Castores pluton reported by Suárez et al. (1985). Site TU89 is just on the northern border of that pluton and this is why the magnetic foliation is mainly E-W (Fig 8c). Site TU88 was drilled on the south-western border of the Santa Rosa pluton and the magnetic foliation is also parallel to the border of the pluton (Fig 8c).

On the other side of the Murray channel, the magnetic fabric is also well-defined at site TU64, CB01 and CB02 with EW foliation and magnetic lineation steeply dipping to the south (Fig 8a, b, c). The magnetic fabric is less intense toward the west (sites CB04 and CB06) with a magnetic foliation oriented NE-SW and similar to the average strike of most tectonic lineaments observed in the area (Fig. 8a, b, c).

In Bahía Fleuriais (sites CB07, CB08) located in the southern edge of Isla Gordon, the magnetic foliation is oriented at nearly 90° from the foliation of the greenschist country rock and the orientation of the Beagle Channel (Fig. 9a, b). The very stable remanent magnetization and especially the large NRM values recorded in the hornblende rich phenocryst rock also indicate the lack of pervasive deformation in these rocks.

Further west, at sites CB09 and CB10, the magnetic foliation is dipping to the NNE and the degree of anisotropy is variable between samples (Fig. 9a, b). At sites CB11, CB12 and CB13, the magnetic foliation is oriented NS with steep dipping magnetic lineation. The degree of anisotropy varies from 1.13 to 1.28 (Fig. 9a, b). Six kilometers to the west, at sites CB14 and CB15 the magnetic foliation is dipping to the west. Along the south arm of the Beagle channel, there is no evidence for tectonic deformation of the plutonic rocks. The magnetic fabric is likely a magmatic fabric acquired during pluton emplacement and probably controlled mainly by the shape of the border of the plutons.

AMS results, in four sites (CB17 to CB20) at the entrance of the O'Brien-Ballenero Channel, indicate a low degree of anisotropy. Sites CB21 and CB22 have a shallow dipping foliation with lineation to the north. Sites from CB24 to CB29 have also low magnetic anisotropy (see auxiliary material table AM_04a).

In Peninsula Brecknock, the three sites (CB31, CB32, and CB33) sampled in the Paleocene intrusive present a well-defined vertical NS magnetic foliation (Fig. 9c). Site CB37 (Fig. 9c) is one of the few sites with a shallow magnetic foliation dipping 30° to the ESE.

The large variation in the degree of anisotropy and orientation of the magnetic ellipsoids is more typical of a magnetic fabric controlled by magmatic processes and strain along the border of the plutons rather than an emplacement under a well-organized tectonic strain field.

5.3.3 Magnetic fabric influence on the remanent magnetization.

The deviation of paleomagnetic vectors from its original direction due to strain deformation and the development of strong magnetic fabrics has been a long standing problem in orogenic belts and other deformed areas (Cogné, 1987, 1988; Lowrie et al., 1986).

In anisotropic material, like some of our samples in intrusive rocks, the characteristic direction might be deviated from the direction of the Earth magnetic field at the time of cooling by 5 to 15°. In paleomagnetic studies at high latitude, this anisotropy could be a serious problem because such deviation may result in large apparent changes in the paleomagnetic declination.

Thus we made (AARM) and (ATRM) experiments in selected samples (20 samples in AARM, 121 samples in ATRM) in order to evaluate and correct possible deviation in the paleomagnetic vector due to the internal magnetic fabric. The results of mean tensor and corrected direction are summarized in Table AM_05 (see auxiliary material) and Table 01 respectively (results of each sample are summarized in Table AM_04b and c, auxiliary data).

Cogné (1987) found a quadratic relation between the AMS and TRM tensor of anisotropy in intrusive rocks with multidomain magnetite, and thus suggested that the AMS

tensor could be used to determine magnetic deviations due to the rock magnetic fabric. We do not find such a simple relation between AMS and anisotropy of remanent magnetization. In our samples, while the AMS is likely controlled by multidomain magnetite, the remanent magnetization, acquired in low fields like TRM and ARM, are mainly carried by single-domain magnetite grains (as shown by SEM observations). The good stability and the high intensity of the ChRMs (> 1 Am^{-1}) at several sites are also evidence of SD magnetite grains as the main carriers of the characteristic remanent magnetizations. In some sites (TU64, CB01) with strong AMS degree (1.5 to 1.7), there is a good agreement between the orientation of the ellipsoids of AMS and those of the ATRM or AARM but the degree of anisotropy of remanent magnetization is much larger (from 1.7 to 2.9) than the AMS one (see auxiliary material Fig. AM_09a). There are sites (CB11, CB13, and CB15) where the AMS fabric and the TRM fabric are similar in both the orientation and degree of anisotropy (see auxiliary material Fig. AM_09b). There are also sites with scattered AMS and ATRM data (see auxiliary material Fig. AM_09c). This last case is mainly found in samples (site CB08, CB18, CB20) with strong remanent magnetizations carried by single domain grains like some samples with large hornblende crystals (see auxiliary material Fig. AM_09c).

We choose to determine TRM or ARM anisotropy tensors especially for sites with high AMS degrees or sites with anomalous directions and with some internal scatter in the distribution of the characteristic directions. The anisotropy tensor was determined for several samples within a site and the inverse anisotropy tensor was used to correct the characteristic direction (Cogné, 1987), as it is often used in archeomagnetism to determine more accurately paleofield vectors (Chauvin et al., 2000; Osete et al., 2015). For samples for which a characteristic plane was determined, all measurements were corrected prior to

the calculation of an anisotropy corrected characteristic plane. For some sites, a characteristic direction was determined on two specimens from the same core (one from thermal demagnetization data and the other from AF demagnetization data). Because the determination of the ATRM or AARM tensors is time consuming since it requires 6 additional measurements, the inverted anisotropy tensor determined in one specimen from one core was, in some cases, used to correct the other specimen of the same paleomagnetic minicore. However, we observe a high variability in the orientation of the ellipsoids and degree of anisotropy between different samples for some sites. Thus, this scatter precludes the possibility to use a mean-site anisotropy tensor to correct the mean-site characteristic direction. The correction was done at the sample level. For some sites, where there is no evidence for a systematic deviation of the direction, and for which the correction was not attempted on all samples, the final mean-site direction was calculated with corrected samples and non-corrected samples (the relative number of corrected versus non-corrected directions is indicated in Table 01).

Correction for anisotropy was applied to 4 sites near the Canal Murray where a strong anisotropy was identified. After correction, there is no scatter in declination with a mean paleomagnetic direction of 316.8, -72.9 and $\alpha 95$ of 4.6°. This result contrasts with the 70° variation in declination (sites TU89 and CB01) observed in the area prior to correction.

At site CB08, the scatter was reduced after correction and the direction is closer to the one observed at site CB07. For sites CB09 to CB15 (~66 Ma), the average direction calculated for the six sites is not changed after applying the anisotropy correction but the scatter between sites and in some cases within sites was reduced after correction.

For the mid-Cretaceous sites located to the west of the Beagle Channel (sites CB17 to CB22) the anisotropy correction was significant only for the two sites CB18 and CB20 with a reduced internal scatter after correction.

Sites CB27, CB28, and CB29 have low anisotropy degrees and we do not apply an anisotropy correction. Sites CB31, CB32 and CB33 have a well-defined AMS fabric but the anisotropy of remanent magnetization was highly scattered. Applying the anisotropy correction resulted in an increased scatter at the site level without significant changes in the mean-site direction. Thus, we calculated a mean direction for the five sites (CB27, CB28, CB29, CB32 and CB33) with a well-defined characteristic direction without anisotropy correction. The mean direction is very well defined with a low angle (3.9°) of confidence at 95% (see Ballenero Brecknock in Table 2; for more details see Table AM_06).

Despite the strong magnetic anisotropy detected for some samples, the numerous experiments carried in this study show that the large apparent counterclockwise tectonic rotations are not the result of a systematic deviation due to magnetic anisotropy.

6.0 Paleomagnetic rotations in Patagonia and their tectonic implications

6.1 The Fueguian rotation pattern

The study area is located at high latitudes and the expected characteristic direction has high inclination. Moreover, the apparent polar wander path (APWP) for South America (Besse and Courtillot, 2002) indicates that South America was located even farther south than its present location during the Late Cretaceous. Thus, a small tilt is likely to induce significant deviation of the declination. A tectonic rotation is thus best evaluated from the

mean direction of a group of individual sites to minimize the effect of undetected tilts than from the direction at a single site. We also do not consider results obtained at site CB16, TU62, CB30 and CB35 because of uncertainties in the age of the magnetization.

The study area is located south of the Darwin Cordillera, which was the place of compressive deformation, strong exhumation and sinistral strike slip tectonics. Despite the expected deformation, the pattern of paleomagnetic directions does not show large scatter due to folding or tilting of the intrusive rocks. On average, normal and reverse polarity directions are antipodal and the deviations of the declinations from the expected ones are best explained by counterclockwise rotations. This observation indicates that the paleomagnetic data can be used to discuss tectonic rotations about vertical axis.

Tectonic rotations at each locality, summarized in Table 2 and Fig. 10, were determined using the Besse and Courtillot (2002) APWP reference curve for South America. Paleomagnetic sites used for calculations at each locality are summarized in Table AM_06 (see auxiliary material), except for Ushuaia Dacite, Jeujepén Pluton, Kranck Pluton and Lemaire Sills which are in Rapalini et al. (2015) and sites from the Magallanes fold and thrust belt which are in Poblete et al. (2014).

Volcanoclastics rocks and sediments from Peninsula Hardy and Navarino Island are remagnetized with an average direction result similar to those found in volcanic sills at Dientes de Navarino (Table 2, Fig. 10). Remagnetization likely occurred in the middle Cretaceous during an event of regional metamorphism associated with the early stages of the closure of the Rocas Verdes basin when part of the Rocas Verdes oceanic crust started to subduct below the arc located to the south-west (Cunningham, 1995; Cunningham et al.,

1991; Klepeis et al., 2010). In Hardy Peninsula, the average paleomagnetic results from remagnetized sites, including those of Cunningham et al. (1991), yield a CCW rotation value of 102.3° ± 20.9° and a very minor inclination flattening of 1.8° ± 7.1° (Table 2; for more details see Table AM_06). The sills at Dientes de Navarino provide a similar result with a CCW rotation value of 105.0°±32.9° and an inclination flattening of 2.4° ± 9.9° (Fig. 10 and Table 2; for more details see Table AM_06).

In the southern arm of the Beagle Channel (Fleuriais Bay) a counterclockwise rotation of 117.8° and an inclination anomaly of -17.8° is observed (no error given since only two sites were used for calculation). In the area of Ballenero and O'Brien Channels, west of the Beagle Channel, the average paleomagnetic result yields a large counterclockwise rotation of 126.8° ± 54.7° and an inclination anomaly of 2.1° ± 15.0°.

The average paleomagnetic result from the 4 sites collected in the intersection area between Murray and Beagle Channel, yields, after anisotropy correction, a CCW rotation of 34.6 ± 13.7 which is lower than the rotation determined with the remagnetized data and other mid-Cretaceous results. Rapalini et al. (2015) have published new paleomagnetic results for the Santa Rosa pluton where site TU88 was sampled. Rapalini et al. (2015) found large changes in declination that were interpreted as evidence for a large relative counterclockwise rotation of the northern part of the Santa Rosa Pluton with respect to its southern part. Since the postulated nearly E-W transcurrent fault does not displace significantly the northern part of the pluton with respect to its southern part, we suggest that a 30° tilt toward the south around a horizontal axis for the northernmost sites might explain the data better than a large relative counterclockwise rotation around a vertical axis. Nonetheless, applying the proposed tilt does not reduce the difference in the magmatic

foliation in the northern and southern part of the intrusive reported by Rapalini et al., 2015. The data of the Santa Rosa pluton presented by Rapalini et al. (2015) were not included with our data of the area because they were not corrected for the effect of the anisotropy.

Rotation and inclination errors for sites located north of the Beagle Channel and previously reported by Rapalini et al. (2015) were recalculated using the Besse and Courtillot (2002) APWP. In particular, results from Lemaire sills were used by combining sites Y2, LC8 and AL8; whereas sites LC9 and AL2 were discarded due to an inclination error larger than 50°.

Paleomagnetic results from ~65 Ma intrusive rocks along the south arm of the Beagle Channel (Cloue Peninsula) provide tectonic CCW rotations of 45.3° ± 19.1° and inclination error of 2.6° ± 5.5° respectively. This rotation value is larger than those found in Cretaceous intrusives from the Beagle-Murray Channel area (Table 2 and Fig. 10).

Paleomagnetic results in Paleocene intrusive show low inclination errors (Table 2) and very similar CCW rotation values: 27.3° ± 23.3 in the Hardy Peninsula (result from only one site) and 26.7° ± 13.3° in the Ballenero-Brecknock locality (Fig. 10).

6.2 Tectonic rotation: small-blocks versus regional block rotation

The major difficulty in the interpretation of the paleomagnetic data is the evaluation of the importance of in situ tectonic rotation of small-blocks versus a large CCW rotation of the Fueguian Cordillera as a rigid body. There are two contrasting models. One corresponds to in situ tectonic rotations of small blocks bounded by left-lateral strike slip faults (Cunningham, 1993). The second model corresponds to an original rectilinear margin

which was bent during the closure of the Rocas Verdes basin (Burns et al., 1980; Dalziel et al., 1973; Kraemer, 2003). A component of rotation due to bending with in-situ block rotation related to Cenozoic wrenching has also been proposed (Diraison et al., 2000).

Cunningham (1993) describes various sets of tectonic structures (ductile foliation in the NW arm of the Beagle Channel) and lineaments (using geomorphological features like fjords). Glasser and Ghiglione (2009) also suggest that fjords correspond to geological structures that have been widened during successive glaciations. Both Cunningham (1993) and Glasser and Ghiglione (2009) argue that the array of structures just reflect evidence of strike-slip deformation, but it is not evident to recognize block rotations. Structural trends like folds axes in the area of Hardy Peninsula and Navarino island and pervasive foliation (red lines in Fig. 10), in the northern part of Navarino Island, have mainly an E-W to ESE-WNW orientation. It is worth noting that folding, block tilting and foliation occurred prior or during the remagnetization event which likely occurred during the first stages of the closure of the Rocas Verdes basin. Thus, the tectonic lineaments have also been rotated and were mainly oriented NS prior to a ~90° CCW rotation. The observed ~90° CCW rotation of the structures is thus best explained by a regional rotation rather than the rotation of small blocks.

To the west, the Fueguian batholith crops out everywhere (Fig. 2) and it is not possible to recognize regional tectonic lineaments like fold axes. Paleomagnetic results from late Cretaceous and Paleocene rocks indicate CCW rotations varying from ~45° to ~25°.

A mechanism of rotation, related to Cenozoic sinistral strike-slip tectonics, should induce tectonic rotations with variable magnitude independently of rock ages from Cretaceous to early Paleogene. In contrast, the observed pattern of tectonic rotations supports a progressive bending of southernmost Patagonia during the late Cretaceous to the early Paleogene, probably during the closure of the Rocas Verdes basin (Burns et al., 1980; Dalziel et al., 1973; Kraemer, 2003). Nonetheless, a small amount of local tectonic rotations induced by strike-slip tectonics cannot be discarded.

Tectonic structures defined by geomorphological lineaments (Cunningham, 1993; Glasser and Ghiglione, 2009) have been attributed to Cenozoic strike-slip tectonics but more field evidences are needed to constrain the nature of the structures and discriminate rotated tectonic foliation of middle Cretaceous ages from Cenozoic brittle structures. The relative coherent results in tectonic rotations and the variable orientation of the magnetic fabric recorded by the plutons do not support major deformation due to Cenozoic strike-slip tectonics south of Darwin Cordillera.

6.3 Tectonic evolution of Southernmost South America and the Antarctic Peninsula

Remagnetization during the middle Cretaceous precludes deciphering the pre-remagnetization tectonic evolution of the area with paleomagnetism. The same limit exists in the Antarctic Peninsula where the Paleozoic and Jurassic rocks have also been remagnetized (Poblete et al., 2011). Paleomagnetic inclinations in middle Cretaceous and Paleocene rocks from the Antarctic Peninsula (Poblete et al., 2011) are also very similar and statistically indistinguishable to the ones found in this study. This observation suggests

that the northern tip of the Antarctic Peninsula and southernmost Patagonia were very close in the middle Cretaceous and late Cretaceous. The Fueguian Andes and the Antarctic Peninsula formed probably a continuous and rectilinear margin at the end of the early Cretaceous period (Fig. 11).

Thus, it is not possible to understand the tectonic evolution of Patagonia without a study of its relation with the Antarctic Peninsula. Gplates software (Earthbyte group) was used to do a set of plate tectonic reconstructions of Patagonia with respect to the Antarctic Peninsula at different times; the reconstruction parameters for the major plates are provided by Seton et al. (2012).

Two tectonic reconstructions have been published recently (Dalziel et al., 2013; Eagles and Jokat, 2014). Unfortunately, Dalziel et al. (2013) did not publish the rotation parameters used in their study and Eagles and Jokat (2014) do not consider the deformation of southern Patagonia. The late Jurassic-early Cretaceous opening of the Weddell Sea and the Rocas Verdes basin will not be discussed because there are numerous uncertainties in plate reconstructions for this area and the available paleomagnetic results do not permit to describe the tectonic evolution of the Rocas Verdes basin during the early Cretaceous. The rotation of the Antarctic Peninsula with respect to East Antarctica is also uncertain before 120 Ma. Most models used for the early opening of the South Atlantic, recently discussed by Heine et al. (2013) imply questionable large intraplate deformation within the South America Plate (Pérez-Díaz and Eagles, 2014) from 138 to 123 Ma. In contrast, there is now a large consensus about the tectonic evolution of the major plates within the South Atlantic ocean after 120 Ma and there is no major difference between the poles of rotation recently proposed by Seton et al. (2012), Heine et al. (2013), Pérez-Díaz and Eagles (2014), Lawver

et al. (2014). Thus, a kinematic evolution of Southern Patagonia from 120 Ma to 40 Ma was done with an Antarctic Peninsula fixed with respect of the East Antarctic plate and without intraplate deformation in South America, except in southern Patagonia. Five reconstructions were made at 120, 100, 80, 60 and 40 Ma (Fig. 11). Continuous magmatic activity in the Fueguian Batholith certainly imply active subduction together with processes such as accretion and erosion, thus the present-day shape of the margin used to construct the block model is obviously schematic.

The remagnetized rocks record a ~100° CCW rotation after ~100 Ma. In the middle Cretaceous, the Rocas Verdes basin was already opened and probably rimmed to the west by a volcanic arc (Fig. 11) (the Navarino microplate from Mpodozis and Rojas (2006)). A detrital zircon U/Pb of ca. 148 Ma in the Yahgan Formation (Klepeis et al., 2010) and observations of Miller et al. (1994) (lateral facies transition from arc deposits into proximal basin fill deposits) and Katz and Watters (1966) (andesitic and basaltic debris from a volcanic arc in the Yahgan Formation) suggest an active magmatic arc related to eastward subduction since the Early Cretaceous. Radiometric ages in igneous rocks indicate contemporaneous magmatic activity along southern Patagonia and the Antarctic Peninsula (Fig. 11). The contemporaneous opening of the Weddell sea and the Rocas Verdes basin suggests that the Navarino block was probably located north of the tip of the Antarctic Peninsula as already proposed in other models (Diraison et al., 2000) (Fig. 2a) rather than to the east of the Antarctic Peninsula as suggested by Dalziel et al. (2013) (Fig. 2b). Also important, the proposed location for the Navarino block can also reconcile the observed rotation in our study and the position of the Antarctic Peninsula, which is constrained by the motion of East Antarctica (Seton et al., 2012; Poblete et al., 2011). In this scenario, the

South Georgia Island is located far away from the Pacific margin, as proposed by Eagles and Jokat (2014).

The westward motion of South America starting just prior 100 Ma resulted in an increase of E-W convergence and the closure of the Rocas Verdes basin was initiated probably by westward subduction of the Rocas Verdes oceanic crust beneath the Navarino block located to the west. Remagnetization within the Navarino block probably occurred during this early stage of deformation characterized by E-W compression within the Navarino block at that time. The final closure of the Rocas Verdes basin which triggered the obduction of the ophiolites onto the South American continent should have occurred prior to 86 Ma (Klepeis et al., 2010) (Fig. 11). About 50° of CCW rotation of the Navarino block should have occurred during this stage (Fig. 11) supporting earlier hypotheses that the tectonic rotation is in part related to the closure of the Rocas Verdes basin (Dalziel et al., 1973; Kraemer, 2003) and obduction processes.

The final collision of the Navarino block with the South American continent (Fig. 11) resulted in the exhumation of the Darwin Cordillera during the Late Cretaceous (Kohn et al., 1995; Maloney et al., 2011; Nelson, 1982) and the propagation of the fold and thrust belt in the Magallanes basin (Klepeis et al., 2010). This deformation was mostly induced by the collision of the Antarctic Peninsula, which acted as a non-rotational rigid block, with Patagonia. In our model this phase of deformation is made of NS shortening north of the Darwin Cordillera but also some sinistral strike-slip displacement of the southernmost blocks from 80 Ma to 40 Ma with respect to South America. According to our model, most of the strike-slip deformation occurred north of the Darwin Cordillera. Paleogene rotations observed in this study to the south of Darwin Cordillera are mostly related to large-scale

block rotation driven by shortening in the Magallanes FTB rather than corresponding to in situ small-block rotations. An example is given by the consistent ~45° rotation recorded in the ca. 65 Ma plutonic rocks to the west of the Beagle channel. Our new paleomagnetic data are consistent with an oroclinal bending of the southernmost blocks during the early stages of deformation, but paleomagnetic results from the MFTB (Maffione et al., 2010; Poblete et al., 2014) indicate that the curvature of the MFTB mainly inherited the curved shape of the craton and the external indenter constituted by the Navarino block. Thus the concept of orocline cannot be used to describe the Patagonian arc as a whole. Instead, the Patagonian arc is best described as a progressive arc from a first stage involving oroclinal bending during the collapse of the Rocas Verdes basin to a final stage related to the development of the MFTB as a primary arc (Poblete et al., 2014).

6.4 Patagonia-Antarctic Peninsula land bridge: Fauna and Climate implications

Dispersal of terrestrial and freshwater vertebrate taxa requires the existence of a link (land bridge or other) between the two end points. Distribution of the genus Madstoia (Albino, 2011) and the egg-laying monotremes (Archer et al., 1985; Pascual et al., 1992) in Australia and South America suggests a biogeographical continuity through Antarctica during the late Cretaceous and early Eocene (Albino, 2011; Dalziel et al., 2013). However, fossil record of ankylosaurs does not support faunal interchange between the Antarctic Peninsula and Patagonia (Salgado and Gasparini, 2006).

Paleogeographic maps providing accurate surface and subsurface boundary conditions are essential for climate models. A land bridge connecting the Antarctic

Peninsula and Patagonia during the Cretaceous through the Paleocene has major impacts in ocean circulation and climate models: If terrestrial and fresh water vertebrate taxa interchange occurred between the Antarctic Peninsula and Patagonia, then deep water interchange between the South Atlantic and the Pacific Oceans was precluded. Cretaceous paleogeography from this area is poorly constrained. Some authors suggest a free way to water interchange between the South Atlantic and Pacific Ocean (Scotese, 2001; Sewall et al., 2007), while others propose a land bridge connecting the Antarctic Peninsula and Patagonia (Blakey, 2008; Markwick and Valdes, 2004).

The observed rotation in the Navarino block suggests a rectilinear margin of the western flank of southernmost Patagonia at least since 120 Ma which was rotated during the closure of the Rocas Verdes basin (Fig. 11). This configuration of Patagonia supports the idea of a land bridge that connected Australia with South America through the Antarctic Peninsula from the middle Cretaceous. The land bridge would have lasted until the final disruption of the Patagonia-Antarctic Peninsula system, marked by the onset of the proto Scotia Sea around 50 Ma (Eagles et al., 2006; Lagabrielle et al., 2009). The hypothesis of a land bridge also limits possible deep-water currents between the South Atlantic Ocean and the Pacific Ocean. Thus, the presence of a Land Bridge should be taken into account for future climate and Gondwana fauna evolution models.

7.0 Conclusions

1. New $^{40}Ar/^{39}Ar$ ages evidence an active mafic magmatism (gabbroic assemblage from Hervé et al. (1984)) from ca. 66 Ma down to 54 Ma, demonstrating that it was not restricted to the early Cretaceous as previously proposed by Suárez et al. (1985).

2. AMS data evidence a strong tectonic fabric in the area of the Murray Channel but only incipient tectonic fabric at other sedimentary sites. Intrusive rocks have variable magnetic fabrics and the variation in the orientation of the ellipsoids do not suggest emplacement of the plutonic rocks under a well-defined regional tectonic strain while shortening was occurring on the northern side of Darwin Cordillera.

3. Paleomagnetic results from early Cretaceous sedimentary and volcaniclastic rocks confirm remagnetization during the mid-Cretaceous as previously suggested by data from Cunningham et al. (1991). Similar results obtained in the Antarctic Peninsula (Poblete et al., 2011) suggest a regional thermo-tectonic event that affected both regions.

4. Our paleomagnetic data show a systematic pattern of counterclockwise rotation with the largest (> 90°) rotations in mid-Cretaceous rocks while late Cretaceous to early Eocene intrusive rocks record ~45° to ~30° CCW rotation. The observation of magnitudes of tectonic rotations with similar magnitudes at a given rock age supports an oroclinal bending of southernmost Patagonia rather than a mechanism of small block rotations related to sinistral strike-slip tectonics.

5. Finally, the observed Fueguian pattern of rotation supports the hypothesis of an oroclinal bending of the Pacific border part of the orogen (including the Navarino block) during the collapse and obduction of the Rocas Verdes basin that occurred before 86 Ma (Klepeis et al., 2010). Rotation continued during the late Cretaceous and the Paleocene, concomitant with the exhumation of the Darwin Cordillera and the advance of the deformational front into the foreland basin (Alvarez-Marrón et al., 1993; Klepeis, 1994b;

Maloney et al., 2011). The curved shape of the Magallanes fold and thrust belt is mainly an inherited shape (Poblete et al., 2014).

Acknowledgments

This is a contribution to Project Anillo Antártico ACT-105 of CONICYT-PBCYT. We thank DIFROL, CONAF and the Chilean Navy for sampling permission. F.P thanks funding from CONICYT and the Institut de Recherche pour le Développement (IRD). We thank Dr. Constantino Mpodozis for the numerous discussions about the geology and geodynamics of southern Patagonia. F.P also thanks Keith Klepeis for inviting him to different field works and fruitful discussions. We also thank Ian Dalziel and reviewers Marco Maffione and Augusto Rapalini for their thorough reviews. We are deeply indebted to M. Calderón and P. Castillo who participated during different fieldworks campaigns. We thank Catherine Kissel and Camille Wandres for their help in the paleomagnetic laboratory of LSCE at Gif/Yvette during Hysteresis data acquisition. We also thank R. Valle (Universidad de Chile) and R. Rivera (Universidad Andrés Bello) who helped with mineral separations. We thank Captain Hugo and the Chonos crew and Captain Keri and Greg from the Northanger for keeping us alive during the sampling seasons.

Reference

Albino, A.M., 2011. Evolution of Squamata Reptiles in Patagonia based on the fossil record. Biol. J. Linn. Soc. 103, 441-457.

Alvarez-Marrón, J., McClay, K., Harambour, S., Rojas, L., Skarmeta, J., 1993. Geometry and evolution of the frontal part of the Magallanes foreland thrust and fold belt (Vicuña area), Tierra del Fuego, Southern Chile. AAPG Bulletin 77, 1904-1921.

Archer, M., Flannery, T.F., Ritchie, A., Molnar, R.E., 1985. First Mesozoic mammal from Australia—an early Cretaceous monotreme. Nature 318, 363-366, doi: 10.1038/318363a0.

Bacon, C.R., 1989. Crystallization of accessory phases in magmas by local saturation adjacent to phenocrysts. Geochimica et Cosmochimica Acta 53, 1055-1066, doi: http://dx.doi.org/10.1016/0016-7037(89)90210-X.

Ballouard, C., Boulvais, P., Poujol, M., Gapais, D., Yamato, P., Tartèse, R., Cuney, M., 2015. Tectonic record, magmatic history and hydrothermal alteration in the Hercynian Guérande leucogranite, Armorican Massif, France. Lithos 220-223, 1-22, doi: 10.1016/j.lithos.2015.01.027.

Barbeau, D.L., Gombosi, D.J., Zahid, K.M., Bizimis, M., Swanson-Hysell, N., Valencia, V., Gehrels, G.E., 2009. U-Pb zircon constraints on the age and provenance of the Rocas Verdes basin fill, Tierra del Fuego, Argentina. Geochem. Geophys. Geosyst. 10, Q12001, doi: 10.1029/2009gc002749.

Barker, P.F., 2001. Scotia Sea regional tectonic evolution: implications for mantle flow and palaeocirculation. Earth-Science Reviews 55, 1-39, doi: 10.1016/s0012-8252(01)00055-1.

Besse, J., Courtillot, V., 2002. Apparent and true polar wander and the geometry of the geomagnetic field over the last 200 Myr. J. Geophys. Res. 107, doi: 10.1029/2000jb000050.

Blakey, R.C., 2008. Gondwana paleogeography from assembly to breakup—A 500 m.y. odyssey, in: Fielding, C.R., Frank, T.D., Isbell, J.L. (Eds.), Resolving the Late Paleozoic Ice Age in Time and Space. Spec. Pap. Geol. Soc. Am., 441, 1-28.

Bruce, R.M., Nelson, E.P., Weaver, S.G., Lux, D.R., 1991. Temporal and spatial variation in the southern Patagonian batholith: constraints on magmatic arc development, in: Harmon, R.S., Rapela, C.W. (Eds.), Andean magmatism and its tectonic setting, Special Paper, Geological Society of America, vol. 265, pp. 1-12.

Bruhn, R.L., Stern, C.R., De Wit, M.J., 1978. Field and geochemical data bearing on the development of a mesozoic volcano-tectonic rift zone and back-arc basin in southernmost South America. Earth Planet. Sci. Lett. 41, 32-46.

Burns, K.L., Rickard, M.J., Belbin, L., Chamalaun, F., 1980. Further palaeomagnetic confirmation of the Magallanes Orocline. Tectonophysics 63, 75-90, doi: 10.1016/0040-1951(80)90108-0.

Calderón, M., Fildani, A., Hervé, F., Fanning, C.M., Weislogel, A., Cordani, U., 2007. Late Jurassic bimodal magmatism in the northern sea-floor remnant of the Rocas

Verdes Basin, southern Patagonian Andes. J. Geol. Soc. London 164, 1011-1022, doi: 10.1144/0016-76492006-102.

Calderón, M., Prades, C., Hervé, F., Avendaño, V., Fanning, C., Massonne, H., Theye, T., Simonetti, A., 2013. Petrological vestiges of the Late Jurassic-Early Cretaceous transition from rift to back-arc basin in southernmost Chile: New age and geochemical data from the Capitán Aracena, Carlos III, and Tortuga ophiolitic complexes. Geochem. J. 47, 201-217.

Carey, S.W., 1958. A tectonic approach to continental drift, in: Carey, S.W. (Ed.), Continental Drift: A symposium ed. University of Tasmania, Hobart, Australia.

Chauvin, A., Garcia, Y., Lanos, P., Laubenheimer, F., 2000. Paleointensity of the geomagnetic field recovered on archaeomagnetic sites from France. Phys. Earth Planet. Inter. 120, 111-136.

Dalziel, I.W.D., de Wit, M.J., Palmer, K.F., 1974. Fossil marginal basin in the southern Andes. Nature 250, 291-294, doi: 10.1038/250291a0.

Cogné, J.P., 1987. TRM deviations in anisotropic assemblages of multidomain magnetite. Geophys. J. R. astr. Soc 91, 1013-1023.

Cogné, J.P., 1988. Strain-induced AMS in the granite of Flamanville and its effects upon TRM acquisition. Geophys. J. 92, 445-453.

Cortés, R., Valenzuela, H., 1960. Estudio Geológico del Área Lago Blanco, Hito XIX, Monte Hope (Porción Sur Central de Tierra del Fuego), Informe Interno. Arch. Téc. Empresa Nac. del Petróleo, Magallanes, Chile., 42 pp.

Cunningham, W.D., 1993. Strike-slip faults in the southernmost Andes and the development of the Patagonian Orocline. Tectonics 12, 169-186, doi: 10.1029/92tc01790.

Cunningham, W.D., 1995. Orogenesis at the southern tip of the Americas: the structural evolution of the Cordillera Darwin metamorphic complex, southernmost Chile. Tectonophysics 244, 197-229, doi: 10.1016/0040-1951(94)00248-8.

Cunningham, W.D., Klepeis, K.A., Gose, W.A., Dalziel, I.W.D., 1991. The Patagonian Orocline: New paleomagnetic data from the Andean Magmatic Arc in Tierra del Fuego, Chile. J. Geophys. Res. 96(B10), 16061-16067, doi: 10.1029/91jb01498.

Dalziel, I.W.D., de Wit, M.J., Palmer, K.F., 1974. Fossil marginal basin in the southern Andes. Nature 250, 291-294, doi: 10.1038/250291a0.

Dalziel, I.W.D., Dott, R.H., Winn, R.D., Bruhn, R.L., 1975. Tectonic relations of South Georgia Island to the Southernmost Andes. Geol. Soc. Am. Bull. 86, 1034-1040, doi: 10.1130/0016-7606(1975)86<1034:TROSGI>2.0.CO;2.

Dalziel, I.W.D., Elliot, D.H., 1972. The Scotia Arc and the Antarctic margin, in: Nairn, A.E.M., Stehli, F.G. (Eds.), The Ocean Basins and margins: I. The South Atlantic. Springer-Verlag US, New York.

Dalziel, I.W.D., Kligfield, R., Lowrie, W., Opdyke, N.O., 1973. Paleomagnetic data from the southernmost Andes and the Antarctandes, in: Tarling, D.H., Runcorn, S.K. (Eds.), Implications of Continental drift to the Earth Sciences. Academic Press, New York, pp. 37-101.

Dalziel, I.W.D., Lawver, L.A., Norton, I.O., Gahagan, L.M., 2013. The Scotia Arc: Genesis, Evolution, Global Significance. Annu. Rev. Earth Planet. Sci. 41, 767-793, doi: 10.1146/annurev-earth-050212-124155.

Day, R., Fuller, M., Schmidt, V.A., 1977. Hysteresis properties of titanomagnetites: Grain-size and compositional dependence. Phys. Earth Planet. Inter. 13, 260-267.

Diraison, M., Cobbold, P.R., Gapais, D., Rossello, E.A., Le Corre, C., 2000. Cenozoic crustal thickening, wrenching and rifting in the foothills of the southernmost Andes. Tectonophysics 316, 91-119, doi: 10.1016/s0040-1951(99)00255-3.

Dott, R.H., Winn, R.D., DeWit, M.J., Bruhn, R.L., 1977. Tectonic and sedimentary significance of Cretaceous Tekenika Beds of Tierra del Fuego. Nature 266, 620-622, doi: 10.1038/266620a0.

Dunlop, D.J., 2014. High-temperature susceptibility of magnetite: a new pseudo-single-domain effect. Geophy. J. Int. 199, 707-716, doi: 10.1093/gji/ggu247.

Eagles, G., Jokat, W., 2014. Tectonic reconstructions for paleobathymetry in Drake Passage. Tectonophysics 611, 28-50, doi: 10.1016/j.tecto.2013.11.021.

Eagles, G., Livermore, R., Morris, P., 2006. Small basins in the Scotia Sea: The Eocene Drake Passage gateway. Earth Planet. Sci. Lett. 242, 343-353, doi: 10.1016/j.epsl.2005.11.060.

Evans, M.E., McElhinny, M.W., 1966. The paleomagnetism of the Modipe Gabbro. J. Geophys. Res. 71, 6053-6063, doi: 10.1029/JZ071i024p06053.

Ferrando, R., Roperch, P., Morata, D., Arriagada, C., Ruffet, G., Córdova, M.L., 2014. A paleomagnetic and magnetic fabric study of the Illapel Plutonic Complex, Coastal Range, central Chile: Implications for emplacement mechanism and regional tectonic evolution during the mid-Cretaceous. J. South Am. Earth Sci. 50, 12-26, doi: 10.1016/j.jsames.2013.11.007.

Fildani, A., Cope, T.D., Graham, S.A., Wooden, J.L., 2003. Initiation of the Magallanes foreland basin: Timing of the southernmost Patagonian Andes orogeny revised by detrital zircon provenance analysis. Geology 31, 1081-1084, doi: 10.1130/G20016.1.

Fosdick, J.C., Romans, B.W., Fildani, A., Bernhardt, A., Calderon, M., Graham, S.A., 2011. Kinematic evolution of the Patagonian retroarc fold-and-thrust belt and Magallanes foreland basin, Chile and Argentina, 51 30'S. Geol. Soc. Am. Bull. 123, 1679-1698, doi: 10.1130/b30242.1.

Ghidella, M.E., Yáñez, G., LaBrecque, J.L., 2002. Revised tectonic implications for the magnetic anomalies of the western Weddell Sea. Tectonophysics 347, 65-86, doi: 10.1016/s0040-1951(01)00238-4.

Ghiglione, M.C., Cristallini, E.O., 2007. Have the southernmost Andes been curved since Late Cretaceous time? An analog test for the Patagonian Orocline. Geology 35, 13-16, doi: 10.1130/g22770a.1.

Glasser, N.F., Ghiglione, M.C., 2009. Structural, tectonic and glaciological controls on the evolution of fjord landscapes. Geomorphology 105, 291-302, doi: 10.1016/j.geomorph.2008.10.007.

Gombosi, D.J., Barbeau Jr, D.L., Garver, J.I., 2009. New thermochronometric constraints on the rapid Palaeogene exhumation of the Cordillera Darwin complex and related thrust sheets in the Fuegian Andes. Terra Nova 21, 507-515, doi: 10.1111/j.1365-3121.2009.00908.x.

Gonzáles-Guillot, M., Escayola, M., Acevedo, R., 2011. Calc-alkaline rear-arc magmatism in the Fuegian Andes: Implications for the mid-cretaceous tectonomagmatic evolution of southernmost South America. J. South Am. Earth Sci. 31, 1-16, doi: 10.1016/j.jsames.2010.11.002.

Grunow, A., 1993. New Paleomagnetic data from the Antarctic Peninsula and their tectonic implication. J. Geophys. Res. 98, 13815-13833, doi: 10.1029/93JB01089.

Halpern, M., Rex, D.C., 1972. Time of folding of the Yahgan Formation and age of the Tekenika Beds, southern Chile, South America. Geol. Soc. Am. Bull. 83, 1881-1886, doi: 10.1130/0016-7606(1972)83[1881:TOFOTY]2.0.CO;2.

Hanes, J.A., York, D., Hall, C.M., 1985. An 40Ar/39Ar geochronological and electron microprobe investigation of an Archean pyroxenite and its bearing on ancient atmospheric compositions. Can. J. Earth. Sci 22, 947-958, doi: 10.1139/e85-100.

Harrison, C.G.A., Barron, E.J., Hay, W.W., 1979. Mesozoic evolution of the Antarctic Peninsula and the southern Andes. Geology 7, 374-378.

Hathway, B., 2000. Continental rift to back-arc basin: Jurassic–Cretaceous stratigraphical and structural evolution of the Larsen Basin, Antarctic Peninsula. J. Geol. Soc. 157, 417-432, doi: 10.1144/jgs.157.2.417.

Heine, C., Zoethout, J., Müller, R.D., 2013. Kinematics of the South Atlantic rift. Solid Earth Discussions 5, 41-116.

Hervé, F., Miller, H., Pimpirev, C., 2005. Patagonia – Antarctica Connections before Gondwana Break-Up, in: Fütterer, D.K., Dmaske, D., Kleinschmidt, G., Miller, H., Tessensohn, F. (Eds.), Antarctica: Contributions to global earth sciences. Springer-Verlag, Berlin, pp. 215-226.

Hervé, F., Pankhurst, R.J., Fanning, C.M., Calderón, M., Yaxley, G.M., 2007. The South Patagonian Batholith: 150 My of granite magmatism on a plate margin. Lithos 97, 373-394, doi: 10.1016/j.lithos.2007.01.007.

Hervé, M., Suárez, M., Puig, A., 1984. The Patagonian Batholith S of Tierra del Fuego, Chile: timing and tectonic implications. J. Geol. Soc. 141, 909-917, doi: 10.1144/gsjgs.141.5.0909.

Jackson, S.E., Pearson, N.J., Griffin, W.L., Belousova, E.A., 2004. The application of laser ablation-inductively coupled plasma-mass spectrometry to in situ U–Pb zircon geochronology. Chem. Geol. 211, 47-69, doi: 10.1016/j.chemgeo.2004.06.017.

Jelínek, V., 1978. Statistical processing of anisotropy of magnetic susceptibility measured on groups of specimens. Stud Geophys Geod 22, 50-62, doi: 10.1007/BF01613632.

Katz, H.R., Watters, W.A., 1966. Geological investigation of the Yahgan Formation (Upper Mesozoic) and associated igneous rocks of Navarino Island, Southern Chile. New

Zealand Journal of Geology and Geophysics 9, 323-359, doi: 10.1080/00288306.1966.10422818.

Klepeis, K.A., 1994a. The Magallanes and Deseado fault zones: Major segments of the South American-Scotia transform plate boundary in southernmost South America, Tierra del Fuego. J. Geophys. Res. 99(B11), 22001-22014, doi: 10.1029/94JB01749.

Klepeis, K.A., 1994b. Relationship between uplift of the metamorphic core of the southernmost Andes and shortening in the Magallanes foreland fold and thrust belt, Tierra del Fuego, Chile. Tectonics 13, 882-904, doi: 10.1029/94tc00628.

Klepeis, K.A., Betka, P., Clarke, G., Fanning, M., Hervé, F., Rojas, L., Mpodozis, C., Thomson, S., 2010. Continental underthrusting and obduction during the Cretaceous closure of the Rocas Verdes rift basin, Cordillera Darwin, Patagonian Andes. Tectonics 29, 1-24, doi: 10.1029/2009tc002610.

Klepeis, K.A., Lawver, L.A., 1996. Tectonics of the Antarctic-Scotia plate boundary near Elephant and Clarence Islands, West Antarctica. J. Geophys. Res. 101, 20211-20231, doi: 10.1029/96JB01510.

Kohn, M.J., Spear, F.S., Harrison, T.M., Dalziel, I.W.D., 1995. 40Ar/39Ar geochronology and P-T-t paths from the Cordillera Darwin metamorphic complex, Tierra del Fuego, Chile. J. Metamorph. Geol. 13, 251-270, doi: 10.1111/j.1525-1314.1995.tb00217.x.

König, M., Jokat, W., 2006. The Mesozoic breakup of the Weddell Sea. J. Geophys. Res. 111, B12102, doi: 10.1029/2005jb004035.

Kraemer, P.E., 2003. Orogenic shortening and the origin of the Patagonian orocline (56° S.Lat). J. South Am. Earth Sci. 15, 731-748, doi: 10.1016/s0895-9811(02)00132-3.

Lagabrielle, Y., Goddéris, Y., Donnadieu, Y., Malavieille, J., Suarez, M., 2009. The tectonic history of Drake Passage and its possible impacts on global climate. Earth Planet. Sci. Lett. 279, 197-211, doi: 10.1016/j.epsl.2008.12.037.

Lawver, L.A., Gahagan, L.M., Dalziel, I.W.D., 2014. Reconstructions of the Southern Ocean and Antarctic regions, in: De Broyer C., K.P., Griffiths H.J., Raymond B., Udekem d'Acoz C. d', et al. (Ed.), Biogeographic Atlas of the Southern Ocean, Scientific Committee on Antarctic Research, Cambridge, pp. 36-42.

Lodolo, E., Menichetti, M., Bartole, R., Ben-Avraham, Z., Tassone, A., Lippai, H., 2003. Magallanes-Fagnano continental transform fault (Tierra del Fuego, southernmost South America). Tectonics 22, 1076, doi: 10.1029/2003TC001500.

Lowrie, W., 1990. Identification of ferromagnetic minerals in a rock by coercivity and unblocking temperature properties. Geophys. Res. Lett. 17, 159-162, doi: 10.1029/GL017i002p00159.

Lowrie, W., Hirt, A.M., Kligfield, R., 1986. Effects of tectonic deformation on the remanent magnetization of rocks. Tectonics 5(5), 713-722, doi: 10.1029/TC005i005p00713.

Ludwig, K.R., 1998. On the treatment of concordant uranium-lead ages. Geochim. Cosmochim. Acta 62, 665-676, doi: 10.1016/S0016-7037(98)00059-3.

Ludwig, K.R., 2001. Isoplot/Ex Version 2.49. A Geochronological Toolkit for Microsoft Excel. Berker Geochronolgy Center, Special Publication 1a, 1-55.

Maffione, M., Speranza, F., Faccenna, C., Rossello, E., 2010. Paleomagnetic evidence for a pre-early Eocene (~50Ma) bending of the Patagonian orocline (Tierra del Fuego, Argentina): Paleogeographic and tectonic implications. Earth Planet. Sci. Lett. 289, 273-286, doi: 10.1016/j.epsl.2009.11.015.

Maloney, K.T., Clarke, G.L., Klepeis, K.A., Fanning, C.M., Wang, W., 2011. Crustal growth during back-arc closure: Cretaceous exhumation history of Cordillera Darwin, southern Patagonia. J. Metamorph. Geol. 29, 649-672, doi: 10.1111/j.1525-1314.2011.00934.x.

Markwick, P.J., Valdes, P.J., 2004. Palaeo-digital elevation models for use as boundary conditions in coupled ocean–atmosphere GCM experiments: a Maastrichtian (late Cretaceous) example. Palaeogeogr. Palaeoclimatol. Palaeoecol. 213, 37-63, doi: 10.1016/j.palaeo.2004.06.015.

McAtamney, J., Klepeis, K., Mehrtens, C., Thomson, S., Betka, P., Rojas, L., Snyder, S., 2011. Along-strike variability of back-arc basin collapse and the initiation of sedimentation in the Magallanes foreland basin, southernmost Andes (53-54.5°S). Tectonics 30, TC5001, doi: 10.1029/2010TC002826.

Miller, C.A., Barton, M., Hanson, R.E., Fleming, T.H., 1994. An Early Cretaceous volcanic arc/marginal basin transition zone, Peninsula Hardy, southernmost Chile. J. Volc. Geoth. Res. 63, 33-58, doi: 10.1016/0377-0273(94)90017-5.

Miller, H., 1983. The position of Antarctica within Gondwana in the ligh of Palaezoic orogenic development, in: Oliver, R.L., James, P.R., Jago, J.B. (Eds.), Antarctic Earth Science. Australian Academy of Sciences, Canberra, pp. 579-581.

Mpodozis, C., Rojas, L., 2006. Orogénesis en los Andes Patagónicos Australes de Tierra del Fuego: Cierre de una "cuenca marginal" o colisión intracontinental?, XI Congreso Geológico Chileno, Antofagasta, Chile, 7 - 11 Aug.

Mukasa, S.B., Dalziel, I.W.D., 1996. Southernmost Andes and South Georgia Island, North Scotia Ridge: Zircon U-Pb and muscovite 40Ar/39Ar age constraints on tectonic evolution of Southwestern Gondwanaland. J. South Am. Earth Sci. 9, 349-365, doi: 10.1016/S0895-9811(96)00019-3.

Nelson, E.P., 1982. Post-tectonic uplift of the Cordillera Darwin orogenic core complex: evidence from fission track geochronology and closing temperature–time relationships. J. Geol. Soc. 139, 755-761, doi: 10.1144/gsjgs.139.6.0755.

O'Neill, C., Müller, D., Steinberger, B., 2005. On the uncertainties in hot spot reconstructions and the significance of moving hot spot reference frames. Geochem. Geophys. Geosyst. 6, n/a-n/a, doi: 10.1029/2004gc000784.

Olivero, E., Malumián, N., 2008. Mesozoic-Cenozoic stratigraphy of the Fuegian Andes, Argentina. Geol. Acta 6, 5-18.

Osete, M.L., Catanzariti, G., Chauvin, A., Pavón-Carrasco, F.J., Roperch, P., Fernández, V.M., 2015. First archaeomagnetic field intensity data from Ethiopia, Africa (1615±12AD). Phys. Earth Planet. Inter. 242, 24-35, doi: 10.1016/j.pepi.2015.03.003.

Pankhurst, R.J., Riley, T.R., Fanning, C.M., Kelley, S.P., 2000. Episodic Silicic Volcanism in Patagonia and the Antarctic Peninsula: Chronology of Magmatism Associated with the Break-up of Gondwana. J. Petrol. 41, 605-625, doi: 10.1093/petrology/41.5.605.

Parada, M.A., Roperch, P., Guiresse, C., Ramírez, E., 2005. Magnetic fabrics and compositional evidence for the construction of the Caleu pluton by multiple injections, Coastal Range of central Chile. Tectonophysics 399, 399-420, doi: 10.1016/j.tecto.2004.12.032.

Pascual, R., Archer, M., Ortiz Jaureguizar, E., Prado, J.L., Godthelp, H., Hand, S.J., 1992. First discovery of monotremes in South America. Nature 356, 704-706, doi: 10.1038/356704a0.

Pérez-Díaz, L., Eagles, G., 2014. Constraining South Atlantic growth with seafloor spreading data. Tectonics 33, doi: 10.1002/2014TC003644.

Poblete, F., Arriagada, C., Roperch, P., Astudillo, N., Hervé, F., Kraus, S., Le Roux, J.P., 2011. Paleomagnetism and tectonics of the South Shetland Islands and the northern Antarctic Peninsula. Earth Planet. Sci. Lett. 302, 299-313, doi: 10.1016/j.epsl.2010.12.019.

Poblete, F., Roperch, P., Hervé, F., Diraison, M., Espinoza, M., Arriagada, C., 2014. The curved Magallanes fold and thrust belt: Tectonic insights from a paleomagnetic and anisotropy of magnetic susceptibility study. Tectonics 33, doi: 10.1002/2014tc003555.

Ramos, V.A., Aleman, A., 2000. Tectonic evolution of the Andes, in: Cordani, U.e.a. (Ed.), Tectonic evolution of South America: Rio de Janerio, Brazil: Proceedings of the 31st International Geological Congress, Rio de Janeiro, Brazil, In-Folio Produçao Editorial, p. 635-685.

Rapalini, A., 2007. A paleomagnetic analysis of the Patagonian Orocline. Geologica Acta 5, 287-294.

Rapalini, A.E., Peroni, J., Luppo, T., Tassone, A., Cerredo, M.E., Esteban, F., Lippai, H., Franciscovilas, J., 2015. Palaeomagnetism of Mesozoic magmatic bodies of the Fuegian Cordillera: implications for the formation of the Patagonian Orocline. Geol. Soc. Spec. Publ., doi: 10.1144/sp425.3

Renne, P.R., Balco, G., Ludwig, K.R., Mundil, R., Min, K., 2011. Response to the comment by W.H. Schwarz et al. on "Joint determination of 40K decay constants and 40Ar∗/40K for the Fish Canyon sanidine standard, and improved accuracy for 40Ar/39Ar geochronology" by P.R. Renne et al. (2010). Geochim. Cosmochim. Acta 75, 5097-5100, doi: 10.1016/j.gca.2011.06.021.

Renne, P.R., Swisher, C.C., Deino, A.L., Karner, D.B., Owens, T.L., DePaolo, D.J., 1998. Intercalibration of standards, absolute ages and uncertainties in $^{40}Ar/^{39}Ar$ dating. Chem. Geol. 145, 117-152, doi: 10.1016/S0009-2541(97)00159-9.

Robion, P., Grelaud, S., Frizon de Lamotte, D., 2007. Pre-folding magnetic fabrics in fold-and-thrust belts: Why the apparent internal deformation of the sedimentary rocks from the Minervois basin (NE — Pyrenees, France) is so high compared to the Potwar basin (SW — Himalaya, Pakistan)? Sedimentary Geology 196, 181-200, doi: 10.1016/j.sedgeo.2006.08.007.

Roddick, J.C., Cliff, R.A., Rex, D.C., 1980. The evolution of excess argon in alpine biotites- A 40Ar-39Ar analysis. Earth Planet. Sci. Lett. 48, 185-208.

Ruffet, G., Feraud, G., Amouric, M., 1991. Comparison of 40Ar-39Ar conventional and laser dating of biotites from the North Trégor Batholith. Geochim. Cosmochim. Acta 55, 1675-1688.

Ruffet, G., Féraud, G., Balèvre, M., Kiénast, J.-R., 1995. Plateau ages and excess argon in phengites: an ^{40}Ar-^{39}Ar laser probe study of Alpine micas (Sesia Zone, Western Alps, northern Italy). Chem. Geol. 121, 327-343, doi: 10.1016/0009-2541(94)00132-R.

Salgado, L., Gasparini, Z., 2006. Reappraisal of an ankylosaurian dinosaur from the Upper Cretaceous of James Ross Island (Antarctica). Geodiversitas 28, 119-135.

Sandwell, D.T., Müller, R.D., Smith, W.H.F., Garcia, E., Francis, R., 2014. New global marine gravity model from CryoSat-2 and Jason-1 reveals buried tectonic structure. Science 346, 65-67, doi: 10.1126/science.1258213.

Scotese, C.R., 2001. Atlas of Earth History, Volume 1, Paleogeography, PALEOMAP Project, Arlington, Texas. 52.

SERNAGEOMIN, 2003. Mapa geológico de Chile, Carta Geol. Chile, Versión Digital, No 4, scale 1:1,000,000. Serv. Nac. de Geol. y Minería, Santiago.

Seton, M., Müller, R.D., Zahirovic, S., Gaina, C., Torsvik, T., Shephard, G., Talsma, A., Gurnis, M., Turner, M., Maus, S., Chandler, M., 2012. Global continental and ocean basin reconstructions since 200Ma. Earth-Science Reviews 113, 212-270, doi: 10.1016/j.earscirev.2012.03.002.

Sewall, J.O., van de Wal, R.S.W., van der Zwan, K., van Oosterhout, C., Dijkstr, H.A., Scotese, C.R., 2007. Climate model boundary conditions for four Cretaceous time slices. Clim. Past 3, 647-657.

Sláma, J., Košler, J., Condon, D.J., Crowley, J.L., Gerdes, A., Hanchar, J.M., Horstwood, M.S.A., Morris, G.A., Nasdala, L., Norberg, N., Schaltegger, U., Schoene, B.,

Tubrett, M.N., Whitehouse, M.J., 2008. Plešovice zircon — A new natural reference material for U–Pb and Hf isotopic microanalysis. Chem. Geol. 249, 1-35, doi: 10.1016/j.chemgeo.2007.11.005.

Smalley, R., Dalziel, I.W.D., Bevis, M.G., Kendrick, E., Stamps, D.S., King, E.C., Taylor, F.W., Lauría, E., Zakrajsek, A., Parra, H., 2007. Scotia arc kinematics from GPS geodesy. Geophys. Res. Lett. 34, doi: 10.1029/2007gl031699.

Smalley, R., Jr., Kendrick, E., Bevis, M.G., Dalziel, I.W.D., Taylor, F., Lauría, E., Barriga, R., Casassa, G., Olivero, E., Piana, E., 2003. Geodetic determination of relative plate motion and crustal deformation across the Scotia-South America plate boundary in eastern Tierra del Fuego. Geochem. Geophys. Geosyst. 4, 1070, doi: 10.1029/2002gc000446.

Stern, C.R., De Wit, M.J., 2003. Rocas Verdes ophiolites, southernmost South America: remnants of progressive stages of development of oceanic-type crust in a continental margin back-arc basin. Geol. Soc. Spec. Publ. 218, 665-683, doi: 10.1144/gsl.sp.2003.218.01.32.

Storey, B.C., 1991. The crustal blocks of West Antarctica within Gondwana: reconstruction and break-up model, in: Thomson, M.R.A., Crame, J.A., Thomson, J.W. (Eds.), Geological Evolution of Antarctica. Cambridge University Press, Cambridge, pp. 587-592.

Suárez, M., Hervé, M., Puig, G.A., 1985. Carta geológica de Chile, 1:250.000. Hoja Isla Hoste e islas adyacentes. XII región. Serv. Nac. de Geol. y Minería 65, 1-113.

Suárez, M., Pettigrew, T.H., 1976. An Upper Mesozoic island-arc-back-arc system in the southern Andes and South Georgia. Geol. Mag. 113, 305-328, doi: 10.1017/S0016756800047592.

Tauxe, L., Watson, G.S., 1994. The fold test: an eigen analysis approach. Earth Planet. Sci. Lett. 122, 331-341, doi: http://dx.doi.org/10.1016/0012-821X(94)90006-X.

Torres Carbonell, P.J., Dimieri, L.V., Olivero, E.B., Bohoyo, F., Galindo-Zaldívar, J., 2014. Structure and tectonic evolution of the Fuegian Andes (southernmost South America) in the framework of the Scotia Arc development. Glob. Planet. Chan., doi: 10.1016/j.gloplacha.2014.07.019.

Turner, G., 1971. 40Ar-39Ar ages from the lunar Maria. Earth Planet. Sci. Lett. 11, 169-191.

Watts, D.R., Watts, G.C., Bramall, A.M., 1984. Cretaceous and Early Tertiary paleomagnetic results from the Antarctic Peninsula. Tectonics 3, 333-346, doi: 10.1029/TC003i003p00333.

Wegener, A., 1929. The Origin of Continents and Oceans, 4th ed. Dover Publications, New York.

Wilson, T.J., 1991. Transition from back-arc to foreland basin development in the southernmost Andes: Stratigraphic record from the Última Esperanza District, Chile. Geological Society of America Bulletin 103, 98-111.

Table and Figure Captions: main text

Table 1: Mean-site paleomagnetic results ordered according to their lithology and location. NN/nn is the number of demagnetized specimens per site and the number of specimens used for calculations of the *in situ* direction. Dec and Inc are declination and inclination of the site-mean ChRM in *in situ* and after tilt correction or anisotropy correction. For sites with anisotropy correction: CC is the number of specimens used for calculations of the corrected direction and cc is the number of specimens with ATRM or AARM correction. For sites with a low number of corrected specimens (cc< 7), the site-mean direction was calculated with corrected and non corrected samples (CC=nn). When cc > 6, the site-mean is only calculated with the anisotropy corrected samples. α95 is the semi-angle at 95% confidence level; K is the Fisher precision parameter; type/age: s/p for secondary/primary magnetization; age is the estimated age of magnetization.

Table 2: Tectonic rotations at each locality shown in Fig. 10. N is the number of sites used for calculation (see auxiliary material AM_06 for details); Latitude/Longitude is the average Latitude/Longitude at each locality; Age is the postulated age of magnetization; Dec_O/E and Inc_O /E is the observed/expected declination and inclination; α95/P95 is the semi-angle of confidence at 95%. Lat_V and Long_V is for latitude/Longitud of the expected Virtual Geomagnetic Pole for stable South America (Besse and Courtillot, 2002). R±dr is the rotation value, and the error at each site. Ei ± dI is the inclination error.

Fig. 1. Physiography of the region showing the principal tectonic plates and structures. The Scotia (SCT) plate is surrounded by the Antarctic (ANT) plate and the South American (SAM) plate. The South Shetland (SSH) and the South Sandwich (SSW) microplates are also depicted. PHX is for the former Phoenix plate. Main structures: MFFZ, Magallanes-Fagnano fault zone; NSR, North Scotia Ridge; SSR, South Scotia Ridge; SFZ, Shackleton Fracture Zone. SGI and SOI are for South Georgia Island and South Orkney Island microcontinents. M/FI is for Malvinas/Falkland Island. Modified from (Barker, 2001; Dalziel et al., 2013; Klepeis and Lawver, 1996; Lagabrielle et al., 2009; Smalley et al., 2007).

Fig. 2. Paleogeographic reconstructions and tectonic evolution of the Patagonia-Antarctic Peninsula system. Reconstructions are from (a) Diraison et al. (2000) and (b) Dalziel et al. (2013). Abbreviations: SAM, South America; AP, Antarctic Peninsula; R.V, Rocas Verdes basin; W.S, Weddell Sea; NI, Navarino Island.

Fig. 3. a) Simplified geological map of the southern tip of South America (modified from (Alvarez-Marrón et al., 1993; Hervé et al., 1984; Klepeis, 1994b; Mpodozis and Rojas, 2006; Olivero and Malumián, 2008; SERNAGEOMIN, 2003; Suárez et al., 1985). Main cities are shown in black circles: 1, Punta Arenas; 2, Ushuaia and 3, Puerto Williams; FL, Fagnano Lake; BC; Beagle Channel; MC, Murray Channel. Legend of the geological maps: 1, Paleozoic Basement; 2, Jurassic magmatism; 3, Cretaceous volcanism; 4, Ophiolitic complexes; 5, Lower Cretaceous sedimentary sequences; 6, mid-Upper Cretaceous sedimentary sequences; 7, Upper Cretaceous-Paleocene sedimentary sequences; 8, Eocene-Pliocene sedimentary sequences; 9, Miocene volcanics; 10, Cretaceous intrusive rocks; 11, Paleocene intrusive rocks; 12, thrust faults; 13, Beagle Channel fault zone; 14,

Magallanes-Fagnano fault zone. Paleomagnetic sampling of this study and previous published paleomagnetic results are shown in white symbols (a, this study; b, Poblete et al., 2014; c, Maffione et al., 2010; d, Rapalini, et al., 2015; e, Cunningham et al., 1991; f, Burns et al., 1980; g, Dalziel et al., 1973). b) Inset showing the area of the Beagle Channel, Isla Navarino and Hardy Peninsula. Color legend is as in Fig. 3a.

Fig. 4. top) $^{40}Ar/^{39}Ar$ age spectra. Apparent age error bars are at the 1σ level; errors in the J-values are not included. Plateau and pseudo-plateau ages (1σ uncertainties) are given when applicable. Inverse isochron (correlation) diagrams, with $^{36}Ar/^{40}Ar$ vs. $^{39}Ar/^{40}Ar$. White ellipses are excluded from isochron regression. Bottom) U/Pb isotopic data on zircons (Tera-Wasserburg Concordia plot), MSWD stands for Mean Squares of Weighted Deviates.

Fig. 5. a) Orthogonal plot of thermal demagnetization in *in situ* coordinates of one sample of the Yahgan Formation (TU5707A) and two samples of the Hardy Formation (TU6006A and TU6104A). b) Orthogonal plot of thermal demagnetization of one sample in a pillow lava. c) XY plot of each component of orthogonal IRM versus temperature (Lowrie, 1990) of sample TU5409 normalized to the maximum value of the soft component. Sampled was saturated along Z/Y/X axis at 2500/250/50 mT respectively (hard/medium/soft coercivity). d) orthogonal plot of thermal demagnetization of one sample drilled in a sill at Dientes de Navarino. e) Equal area stereonet of site mean ChRMs from the Yahgan Formation (triangle), Hardy Formation (circle) and pillow lavas of the Tortuga Ophiolite (square). IS, TC for *in situ*, tilt corrected directions. Open blue/black symbols represents results from this study/Cunningham et al. (1991). f) Fold tests according to Tauxe and Watson (1994) indicating magnetization acquired after tilting. Dashed blue

lines are 95% confidence bounds. Solid line is the cumulative distribution of the % untilting required to maximize tau (maximum eigenvalue). Graphics and calculations were done with L. Tauxe's PmagPy-2.51 software package. g) Equal area stereonet of site mean ChRMs from sites drilled in sills at Dientes de Navarino. IS/TC are the *in situ*/tilt corrected results. For orthogonal plots, *n situ* (IS) orthogonal plot of thermal demagnetization (TH) of one sample drilled in a sill at Dientes de Navarino. solid/open circles correspond to projection onto the horizontal/vertical plane. For stereonets, open symbols correspond to negative inclination.

Fig. 6: a, b, c, d, e) Orthogonal plots in *in situ* coordinates of thermal demagnetization of samples in intrusive rocks. Solid/Open circles correspond to projection onto the horizontal/vertical plane. f) Equal area stereonet of site mean ChRMs in intrusive rocks. Open/Solid symbols are for negative/positive inclinations. We have grouped the site mean ChRMs according to the age of the magnetization; at a given age the color of the symbols represents the sampled area. The black/color stars are the expected/average result for each age/locality.

Fig. 7. a) Plot of the mean-site AMS data foliation (green) onto the Shaded relief map (Shuttle Radar Topography Mission Data SRTM1). Structural lineations are depicted in red. b) T-P' diagram showing the difference of the degree of anisotropy in the region; each dot represents one sample. c) Equal area projection of the kmin and kmax directions of the AMS ellipsoids in *in situ* coordinates.

Fig. 8. a) Plot of the mean-site AMS foliation (green) onto the shaded topography (SRTM data). Magmatic/Geomorphologic lineaments are depicted in red/blue. b) T-P'

diagram. c) Equal area projection of the AMS ellipsoids in *in situ* coordinates. Thick lines out of the AMS stereonet are the strikes of the mean lineaments recognized at each area.

Fig. 9. a) Plot of the mean-site AMS foliation (green) onto the shaded topography (SRTM data). Geomorphologic lineaments are depicted in red/blue. b) Equal area projection of the AMS tensor and T-P' diagrams for sites 07 to 15. c) Equal area projection of the AMS tensor and T-P' diagrams per sample for sites 31, 32, 33 and 37.

Fig. 10. Compilation of tectonic rotations in the Fueguian Andes and the Magallanes fold and thrust belt. Arrows are tectonic rotations determined from the ChRMs. The rotation angle is the angle between the black line and the arrow. Red lines in Navarino Island and Hardy Peninsula are structural trends.

Fig. 11. Plate reconstructions for Patagonia and the Antarctic Peninsula between the mid-Cretaceous and the late Eocene. Reconstruction were made using the Gplate software and the plate circuit from Seton et al. (2012) and the moving IAHS frame of O'Neill et al. (2005). Rotations Poles for the new blocks defined in Patagonia were calculated interactively with the Gplate software. Lines with filled triangles represent subduction zones. SO and SG correspond respectively to South Orkney and South Georgia islands. The dashed line corresponds to an expected deformation zone (not discussed in this study). The oceanic crust is shown with the gravimetric data of Sandwell et al. (2014). In the Weddell Sea, part of the oceanic crust has been subducted and replaced by the Scotia oceanic crust. However, because the present-day remnant Weddell crust is mainly the one attached to the Antarctic continent, the other symmetrical part of the Weddell Sea is shown by the reconstructed isochrons (thin black lines). The formation of the Rocas Verdes basin is

contemporaneous with the early opening of the Weddell Sea. The red circles correspond to points with radiometric ages in volcanic and intrusive rocks emplaced within a 10 Myr window prior to the time of each reconstruction. This delineates an active magmatic arc along the western margin of the Antarctic Peninsula and Southern Patagonia.

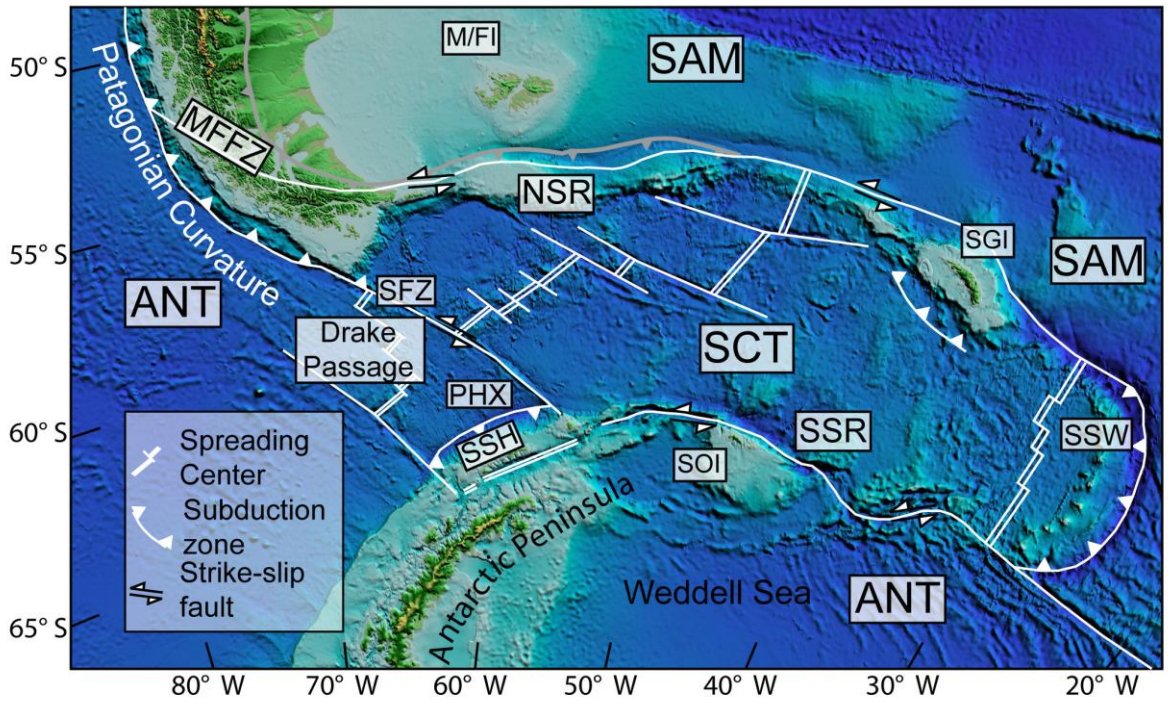

Figure 1

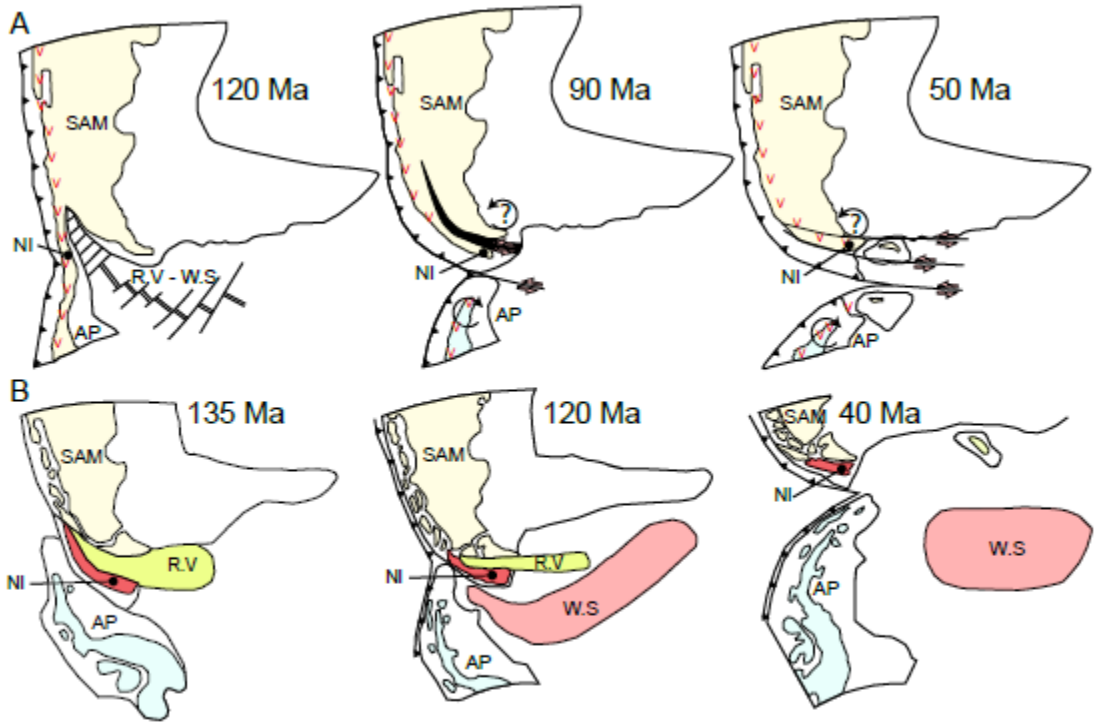

Figure 2

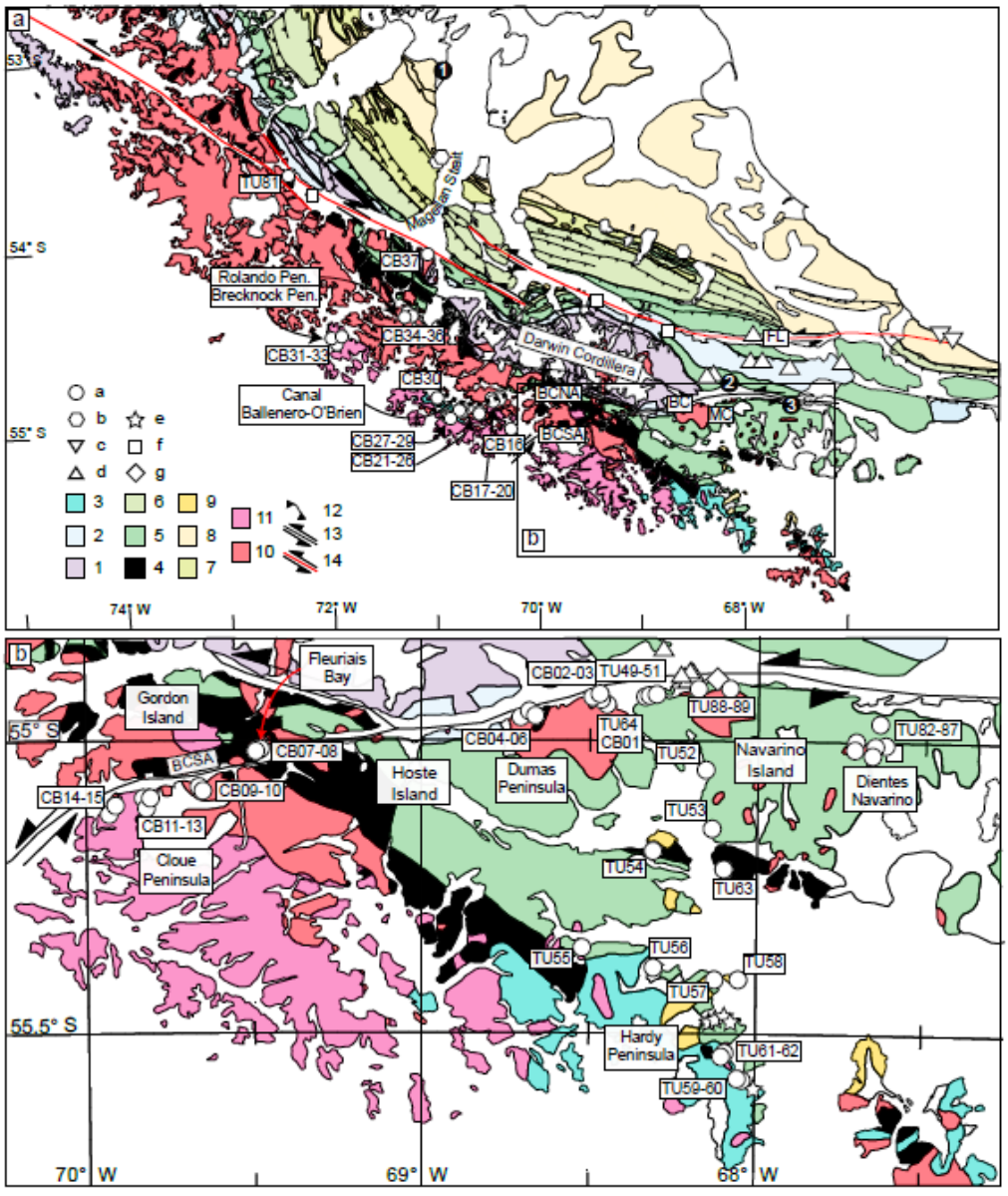

Figure 3

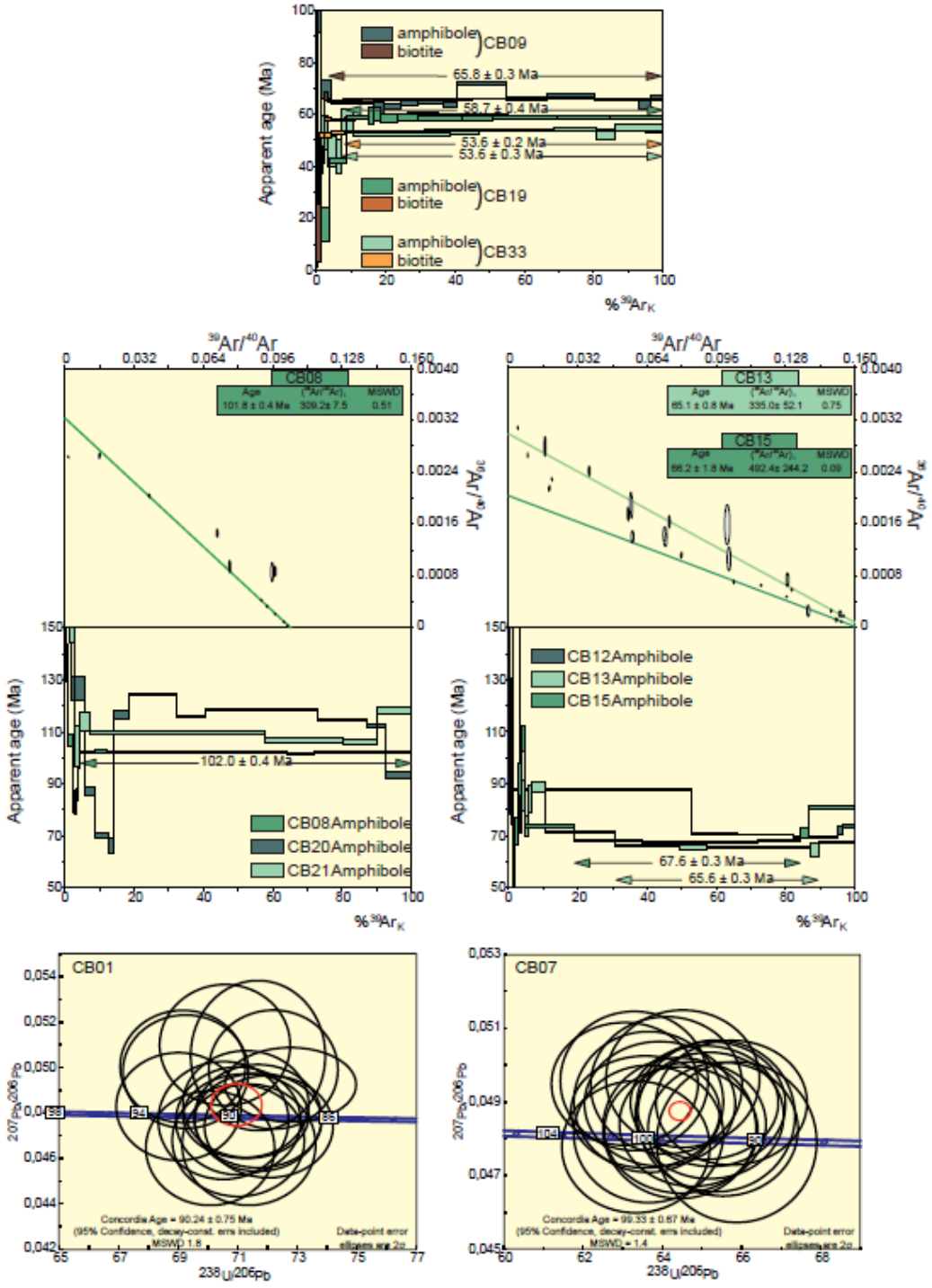

Figure 4

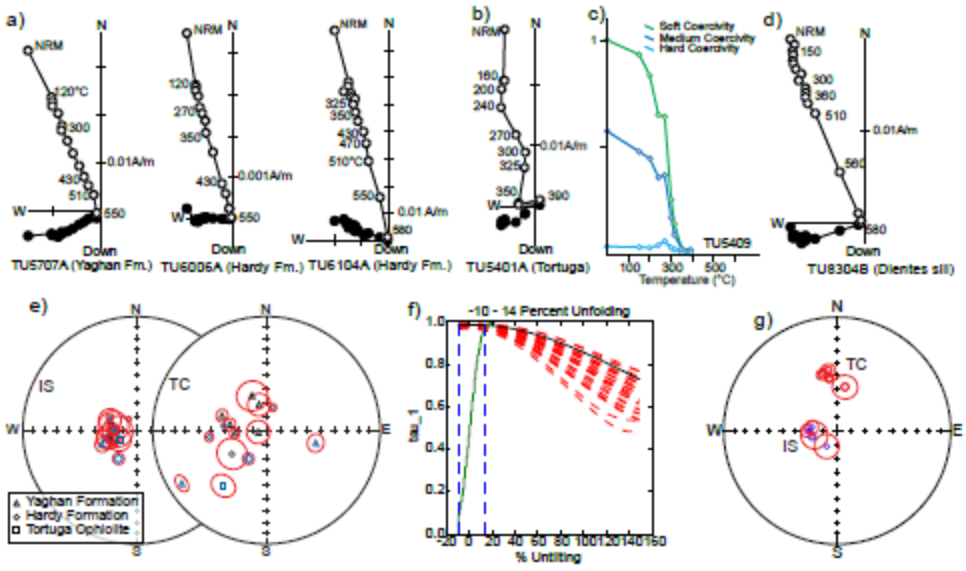

Figure 5

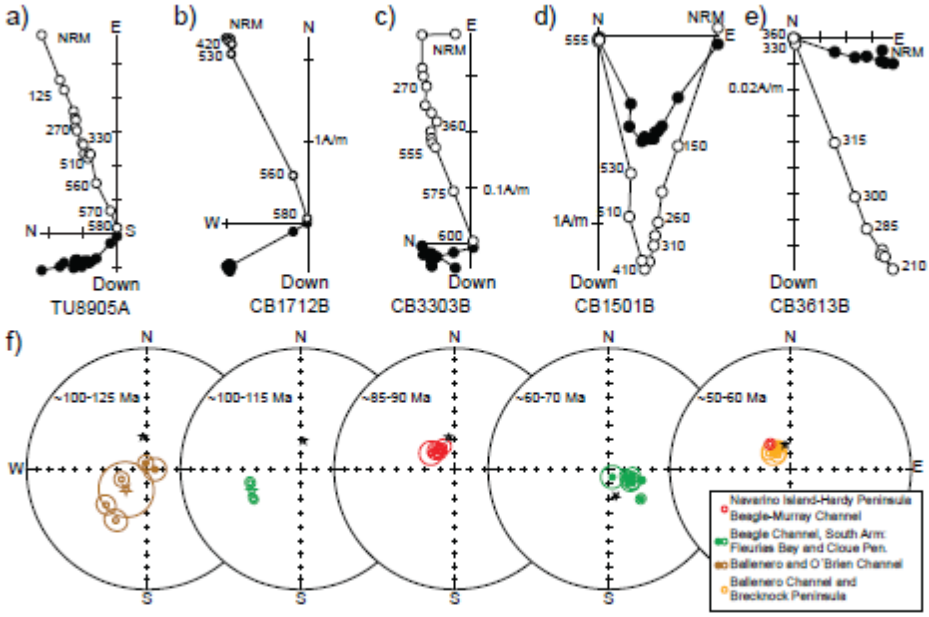

Figure 6

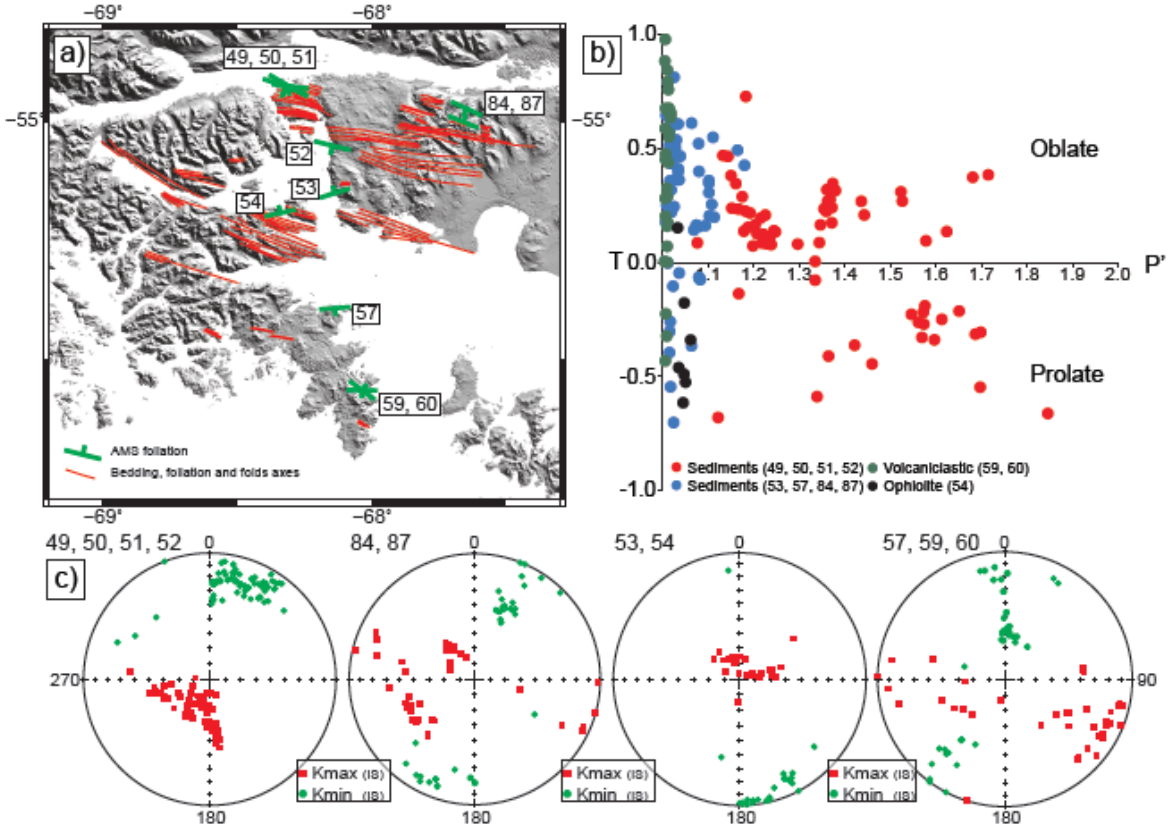

Figure 7

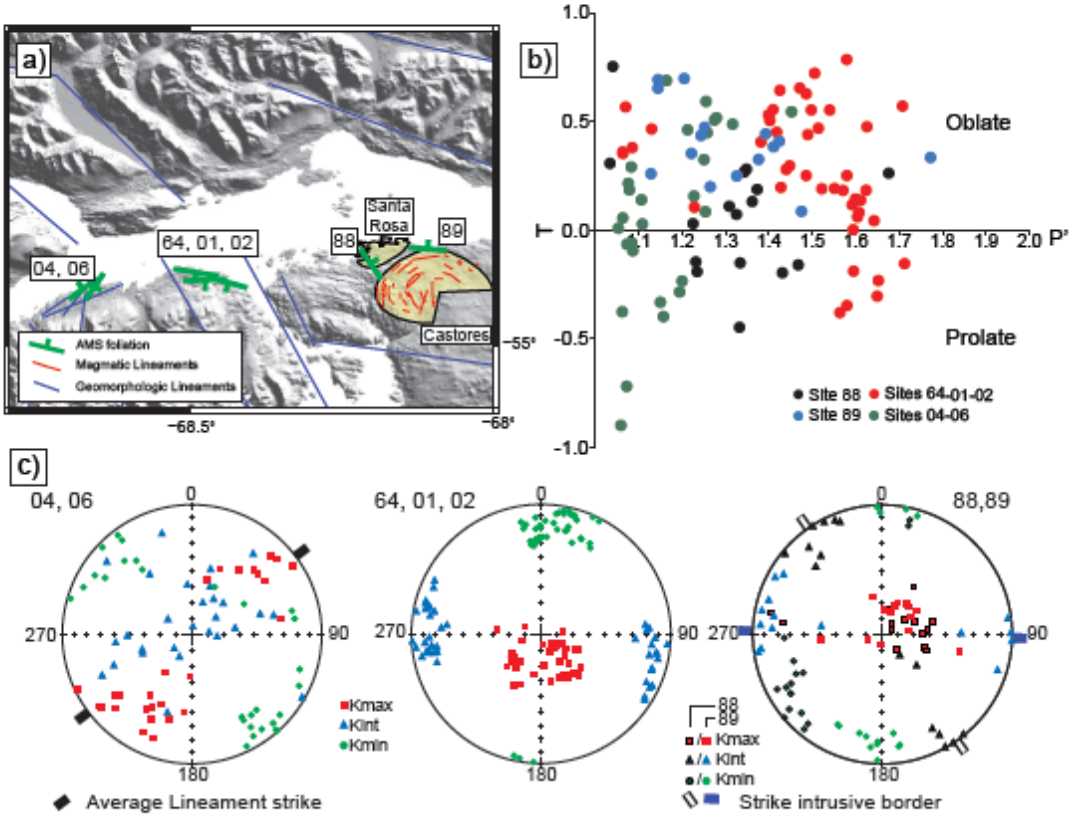

Figure 8

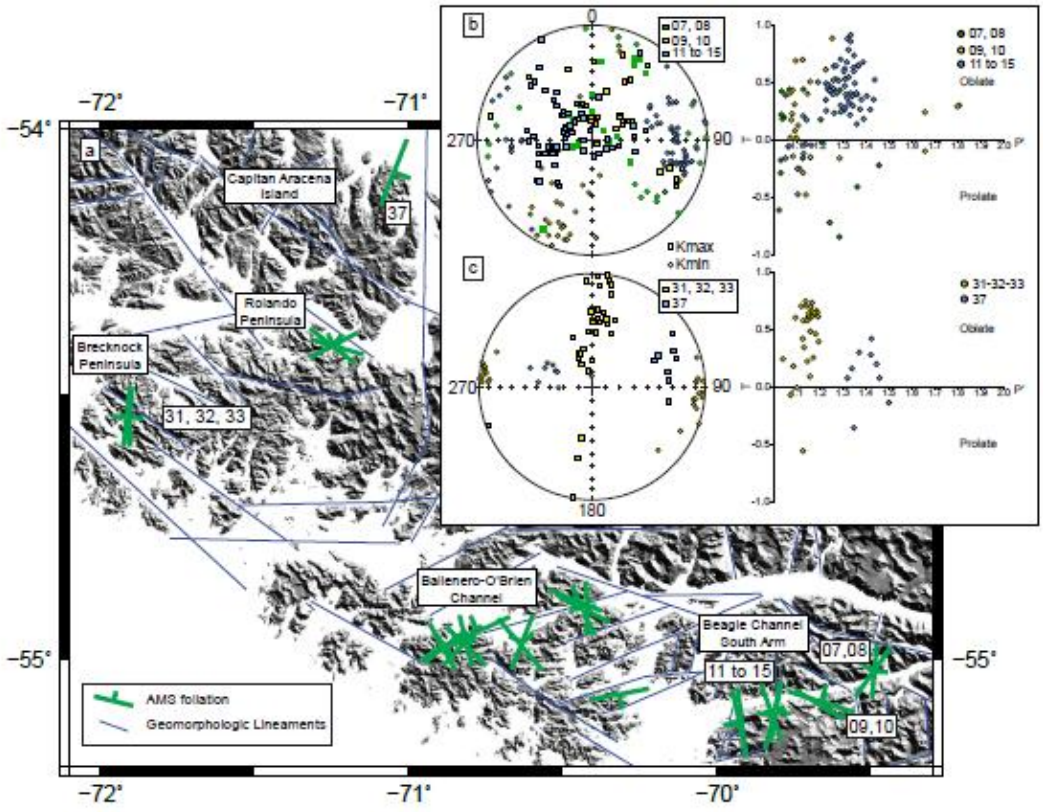

Figure 9

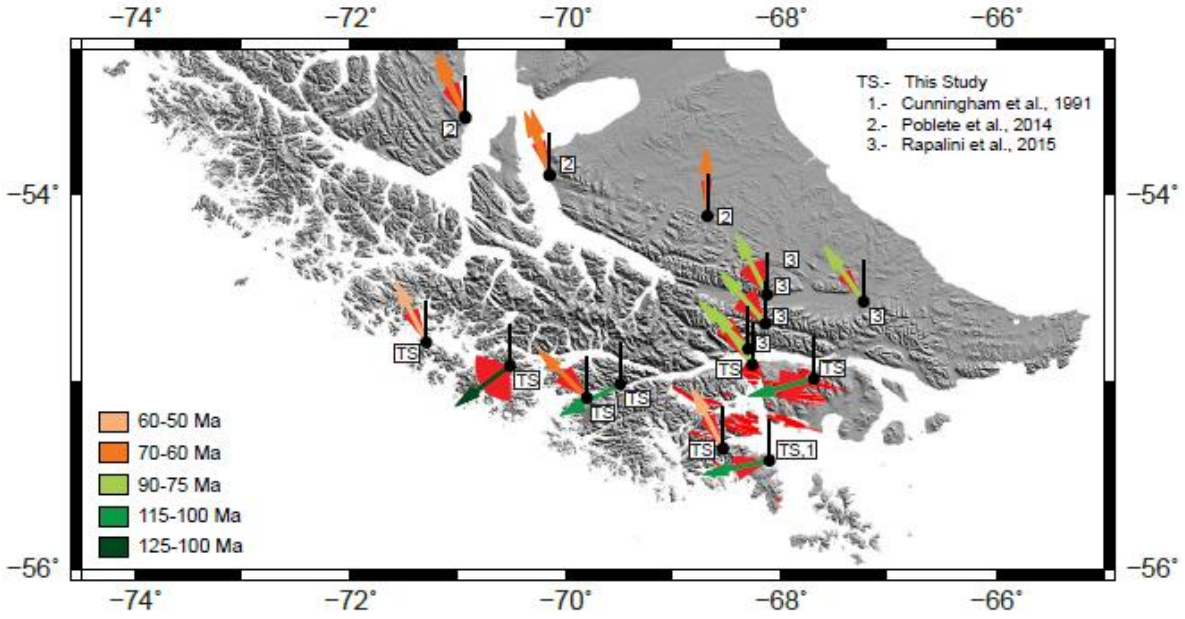

Figure 10

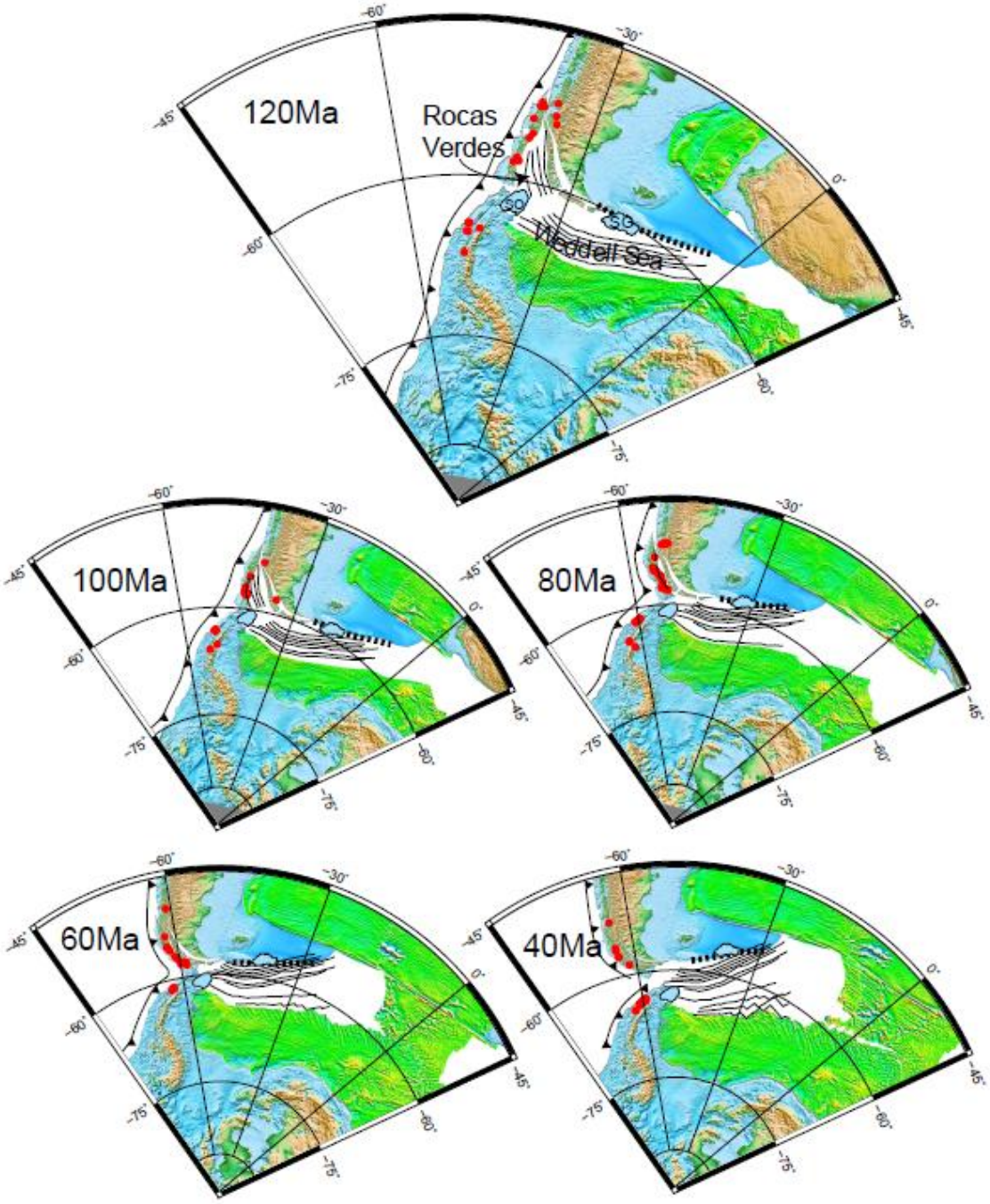

Figure 11

Table 01: Paleomagnetic results

Sills and sedimentary, interbedded volcanic and ophiolitic rocks: Navarino Island and Hardy Pen.

Location	Site	Lithology	NN/nn	In Situ		Tilt Corrected		a95	Kappa	Type/Age
				Dec	Inc	Dec	Inc			
Dientes N.	TU82	Sill	11/04	214.2	-76.4	10.1	-57.8	8.8	111	S /~100-115
Dientes N.	TU83	Sill	17/17	257.4	-71.5	351.2	-51.5	2.6	188	S /~100-115
Dientes N.	TU85	Sill	10/10	269.6	-68	345.5	-47.5	4.2	142	S /~100-115
Dientes N.	TU86	Sill	09/05	277.8	-71.8	351.5	-45.1	4.8	257	S /~100-115
Navari. I.	TU53	sandstone	14/09	255.1	-66.5	104.5	-52.9	6.2	82.5	S /~100-115
Pasteur P.	TU54	Pillow Lava	08/04	241.7	-76	217.8	-37.9	8.3	123.7	S /~100-115
Hardy Pen.	TU57	Sandstone	09/07	246.9	-63	237.8	-12.9	5.1	143.3	S /~100-115
Hardy Pen.	TU59	Volcaniclas.	13/08	325.6	-80.2	275.7	-59	1.4	1660.6	S /~100-115
Hardy Pen.	TU60	Volcaniclas.	12/07	270.8	-73.6	263.3	-47.9	3.3	340.5	S /~100-115
Hardy Pen.	TU61	Volcaniclas.	16/10	295.3	-68.8	16.1	-73.1	2.7	284.4	S /~100-115
Navari. I.	TU63	Sheeted D.	13/09	212.2	-65.8	-----	-----	---	-----	S /~100-115
Hardy Pen.	5161*	Sedimentary	18/18	246.6	-71.9	264.3	-67	3.6	246.6	S /~100-115
Hardy Pen.	5162*	Sedimentary	12/12	290.5	-69.5	344.1	-70.9	8.1	290.5	S /~100-115

Hardy Pen.	5181*	Sedimentary	13/13	251.4	-70.8	279.4	-63.4	4.2	251.4	S /~100-115
Hardy Pen.	5191*	Sedimentary	14/14	271.8	-73.2	288.4	-56.1	4.3	271.8	S /~100-115
Hardy Pen.	551*	Sedimentary	18/18	256.1	-69.1	257.5	-84	8.3	256.1	S /~100-115
Hardy Pen.	593*	Sedimentary	11/07	278.9	-73	337.5	-63.1	10.9	278.9	S /~100-115
Hardy Pen.	5182*	Pyroclastic	08/08	266.3	-76.4	235.4	-59.8	10.9	266.3	S /~100-115

*: from Cunningham et al., 1991.

Intrusive Rocks: Navarino Island and Hardy Peninsula

			In Situ					AARM/ATRM Corrected					
Location	**Site**	**Lithology**	**NN/nn**	**Dec**	**Inc**	**a95**	**Kappa**	**CC/cc**	**Dec**	**Inc**	**a95**	**Kappa**	**Type/Age**
Beagle C.	TU64	Granite	09/07	311.5	-74.5	4.7	178.1	07/--	314.2	-72.3	5.8	114.6	P /~85-90 Ma
Beagle C.	TU88	Intrusive	15/10	300.1	-69.6	5.8	71.5	07/07	303.7	-70.6	8	58.3	P /~85-90 Ma
Beagle C.	TU89	Intrusive	15/13	280.6	-77.3	5	70.3	10/10	318.2	-74.6	4.6	109.9	P /~85-90 Ma
Beagle C.	CB01	Tonalite	15/11	349.8	-77.2	6.1	57.8	09/09	333.2	-73	5	108.5	P /~85-90 Ma
Hardy Pen.	TU55	Tonalite	08/08	320.3	-68.2	3.5	178	--/--	--/--	-----	-----	---	P /~50-60 Ma
Intrusive Rocks: Beagle Channel-southwest arm													
Fleuriais B.	CB07	Granodiorite	0/08	237.9	-52	2.9	285	--/--	-----	-----	---	-----	P /~100-115 Ma
Fleuriais B.	CB08	Horblendite	10/10	263.2	-55.5	6.4	57.6	10/04	254.9	-54	3.5	196.2	P /~100-115 Ma
Cloue P.	CB09	Gabbro-dior.	10/06	83.1	76.9	4.8	192.7	06/04	104.4	74.7	4.6	216.2	P /~60-70 Ma
Cloue P.	CB10	Granite	11/10	115.9	70.9	5.1	90.3	10/06	120.1	71.6	4.6	113.2	P /~60-70 Ma
Cloue P.	CB11	Tonalite	16/15	111.6	75.5	1.7	521.3	15/15	109.9	67.2	2.4	149.6	P /~60-70 Ma
Cloue P.	CB12	Gabbro-dior.	11/11	119.1	76.8	4.3	143.6	11/06	121.6	75.1	4.2	119.6	P /~60-70 Ma
Cloue P.	CB13	Gabbro-dior.	11/11	114.9	75.8	3.4	186.6	11/10	113.1	77.6	4.2	116.8	P /~60-70 Ma
Cloue P.	CB14	Tonalite	11/09	212.9	82.4	9.2	32.5	09/08	157.9	84.1	7.7	45.9	P /~60-70 Ma

Cloue P.	CB15	Tonalite	11/11	142.7	61.8	5.5	69.6	11/09	133.9	60.5	3.8	145.3	P /~60-70 Ma
Intrusive Rocks: Ballenero and O'Brian Channel													
O'Brian C.	CB17	Gabbro	18/13	255.9	-72.4	5	70.7	13/08	248.3	-71.3	5	70.8	P /~100-125 Ma
O'Brian C.	CB18	Hrbl. Gabbro	15/15	58.6	85.2	8.4	21.7	11/11	93.3	84.8	7.6	37.4	P /~100-125 Ma
O'Brian C.	CB20	Hornblendite	10/09	318	77.2	8.9	34.6	08/08	345	85.9	5.2	113.4	P /~100-125 Ma
Ballenero C.	CB21	Hrbl. Gabbro	12/12	224.5	-53.1	7.8	32	12/05	228.9	-52.6	6.5	46.2	P /~100-125 Ma
Ballenero C.	CB22	Tonalite	09/06	207.7	-45.7	5.6	141.7	06/05	211.5	-48.6	7.5	81.4	P /~100-125 Ma
Intrusive Rocks: Ballenero Channel and Brecknock Peninsula													
Ballenero C.	CB27	Dike	10/07	305.5	-71.8	4.5	183.8	--/--	-----	-----	---	-----	P /~50-60 Ma
Ballenero C.	CB28	Granite	07/05	317.5	-77.3	4.9	244.8	--/--	-----	-----	---	-----	P /~50-60 Ma
Ballenero C.	CB29	Granodiorite	10/09	332.5	-72.5	3.5	220.4	--/--	-----	-----	---	-----	P /~50-60 Ma
Brecknock P.	CB32	Tonalite	13/07	313.9	-74.2	8.3	53.5	--/--	-----	-----	---	-----	P /~50-60 Ma
Brecknock P.	CB33	Tonalite	13/09	334.5	-73.7	3.1	279.4	--/--	-----	-----	---	-----	P /~50-60 Ma

Intrusive Rocks: Unknown age

				In Situ		Tilt Corrected				
Location	**Site**	**Lithology**	**NN/nn**	**Dec**	**Inc**	**Dec**	**Inc**	**a95**	**Kappa**	**Type/Age**
O'Brian C.	CB16#	Dike	08/07	210.9	83.3	-----	-----	5.5	123.3	p /Unknown
Hardy Pen.	TU62#	Diorite	09/05	195.5	-80.2	-----	-----	5.3	209	u /Unknown
Ballenero C.	CB30#	Int/Volc	--/14	48.4	82.4	69.2	39.0	4.9	69.2	u /Unknown
Ballenero C.	CB30#	Int/Volc	--/09	315.5	-74.9	269.8	-37.2	3.2	266.9	u /Unknown
Rolando. P.	CB35*#	Granodiorite	31/08	89	64.9	-----	-----	5	125.9	p /Unknown

13CB35* result using samples from sites CB35 and CB36

#: discarded results, see text for explanation

Table 02: Paleomagnetic rotations (see Table AM 06 for sites used at each locality)

Results with an attributed age of 125-100 Ma															
Locality	**N**	**Latitud**	**Longitud**	**Age**	**Dec O**	**Inc O**	**A95**	**Dec E**	**Inc E**	**Lat V**	**Long V**	**P95**	**R±dr**	**Ei±dI**	**Reference**
Ballenero-Obrien C.	5	-54.928	-70.517	120	225.7	-69.9	18.6	352.5	-67.8	83.9	238.5	3.1	-126.8 ±54.7	2.1±15.0	TS
Results with an attributed age of 115-100 Ma															
Dientes Navarino	4	-54.999	-67.694	100	258.8	-73.2	9.7	3.8	-70.8	87.8	29.2	11.5	-105.0 ±32.9	2.4±9.9	TS
Hardy Pen (Remag)	14	-55.433	-68.108	100	261.6	-72.9	4.6	3.9	-71.1	87.8	29.2	11.5	-102.3 ±20.9	1.8±7.1	TS, 1
BCSA (Fleurais)	2	-55.026	-69.493	100	246	-53.1	----	3.8	-70.9	87.8	29.2	11.5	-117.8 ±----	-17.8±---	TS
Results with an attributed age of 90-75 Ma															
Beagle - Murray Channel	4	-54.923	-68.268	90	316.8	-72.9	4.6	351.4	-72	84.8	175.8	3.6	-34.6± 13.7	0.9±4.1	TS
Ushuaia Dacite	3	-54.839	-68.304	75	303.5	-66.9	6.9	349.7	-72.5	83.6	170.6	7.2	-46.2± 18.0	-5.6±6.6	3
Jeujep	5	-	-	75	314.5	-33.6	4.5	349.9	-72.4	83.6	170.6	7.2	-	-	3

én Pluton		54.584	67.233										35.4± 11.7	38.8± 5.1	
Kranc k Pluton	7	-54.547	-68.131	75	322.9	-51.8	16.5	349.8	-72.3	83.6	170.6	7.2	-26.9± 24.4	-20.5± 13.7	3
Lemai re Sills	3	-54.703	-68.144	75	309	-62.9	12.1	349.8	-72.4	83.6	170.6	7.2	-40.8± 24.5	-9.5±1 0.3	3
Results with an attributed age of 70-60 Ma															
BCSA Cloue Pen	7	-55.1	-69.805	65	300.7	-73.4	6.4	346	-70.8	82	193.7	3.6	-45.3± 19.1	2.6±5. 5	TS
Results with an attributed age of 60-50 Ma															
Ballen ero Breck nock	5	-54.804	-71.295	60	320.8	-74.2	3.9	347.5	-72.7	82.4	168.5	4.3	-26.7± 13.3	1.5±3. 8	TS
Hardy Penins ula	1	-55.37	-68.538	60	320.3	-68.2	3.5	347.6	-73.2	82.4	168.5	4.3	-27.3± 23.3	-5.0±--	TS
Results from the Magallanes fold and thrust belt. Attributed age of 70-60 Ma															
Bruns wick TU95	1	-53.574	-70.937	65	143.6	76.2	3.1	166.5	69.7	82	193.7	3.6	-22.9± 11.6	6.5±3. 2	2
Bruns wick TF10	1	-53.582	-70.93	65	140.2	69.8	6.1	166.5	69.7	82	193.7	3.6	-26.3± 15.1	0.1±5. 3	2
White side TU45	1	-53.896	-70.148	65	144.6	70.3	3.1	166.5	69.8	82	193.7	3.6	-21.8± 8.9	0.3±3. 1	2
White side TU74	1	-53.897	-70.151	65	151	64.7	3.7	166.5	69.8	82	193.7	3.6	-15.4± 8.5	5.3±3. 5	2
T del	1	-	-	65	344.7	63.4	3.9	346.3	-70.3	82	193.7	3.6	-	6.9±3.	2

Fuego TU28		54.119	68.684										1.6±8.6	7	

BCSA: Beagle Channel South Arm

Refereces:
TS. This Study
1. Cunningham et al., 1991.
2. Poblete et al., 2014
3. Rapalini et al., 2015

Highlights

- New $^{40}Ar/^{39}Ar$ ages indicate mafic magmatism during the Paleocene.
- CCW rotations larger than 90° are recorded in the Fueguian Andes.
- The Fueguian pattern of rotation supports the hypothesis of oroclinal bending.
- A tectonic evolution of Patagonia and the Antarctic Peninsula is proposed.